Method of spectral response to stochastic processes for measuring the nonreciprocal effective interactions

E. A. Sametov, E. A. Lisin, and O. S. Vaulina
Joint Institute for High Temperatures, 125412 Moscow, Russia
and Moscow Institute of Physics and Technology, 125412 Moscow, Russia

(Received 16 June 2023; accepted 13 October 2023; published 17 November 2023)

The theoretical background of the nonperturbative method of spectral response to stochastic processes (SRSP) for measuring the nonreciprocal interparticle effective interactions in strongly coupled underdamped systems is described. Analytical expressions for vibrational spectral density of confined Brownian particles with a nonreciprocal effective interaction are presented. The changes in the vibrational spectral density with varying different parameters of the system (nonreciprocity, viscosity, ratios of particle sizes, and intensities of random processes acting on each particle) are discussed using the example of a pair of nonidentical particles in a harmonic trap. The SRSP method is compared to three other nonperturbative methods. The SRSP method demonstrates an undeniable advantage when processing particle trajectories with errors in particle tracking.

DOI: 10.1103/PhysRevE.108.055207

I. INTRODUCTION

A violation of the action-reaction symmetry in systems of a different nature has recently become a hot topic of multiple interdisciplinary studies [1–25]. On the mesoscopic length scale, Newton's third law can be formally broken when the interactions between particles are mediated by a nonequilibrium environment which is also effectively taken into account by means of dissipative forces and particle energy. Striking examples of such systems are catalytically active [9,11,14,26–28] and flowing [2,29–33] colloidal suspensions where the nonreciprocity (asymmetry) of interaction may occur due to diffusiophoretic forces acting on Janus particles [25–27] and particles in colloidal mixtures [9,11,16], and due to depletion forces [29–32] acting on closely spaced macroparticles moving through a colloidal dispersion. Examples also include charged microparticles in colloidal plasmas (also called complex or dusty plasmas) [1,6,7,24,34–37] which can interact nonreciprocally due to different dielectric properties of the particles [38], due to shadowing of ion or neutral gas fluxes [39–41] towards one particle by another one that differs in size [42], and due to wake-mediated forces generated by the flow of ions past particles [17,43–46]. The nonreciprocity of interaction (interaction symmetry breaking) can significantly affect self-organization, self-assembly, mass transfer, energy redistribution, and nonequilibrium phase transitions.

The study of the nonreciprocal effective interactions is a complicated experimental task. In colloidal plasmas, pair interparticle interactions are typically explored in two-particle systems, because the consideration of collective effects is not required. Most existing methods require a special modification of an experimental setup [43,47–52], preliminary measurements of external forces acting on particles [49], and/or prior information on environment parameters and the law of interparticle interaction [47,48,53]. An external perturbation of a particle system is a common approach for exploring the nonreciprocal interactions in colloidal plasmas. It can be caused by laser manipulations [43,48–51], or by a low-frequency modulation of the electrode bias [47], or by using a gravity-driven dynamic probe [52]. Analyzing the dynamic response of the particles to the external perturbation makes it possible to determine the interaction forces between one pair of particles [43,49,50,52] and to evaluate whether the interaction in a many-particle system is nonreciprocal or not [48]. In addition to the requirements mentioned above, external perturbations can lead to appreciable changes in the investigated system.

Most nonperturbative methods lack the requirements and drawbacks listed above [54–60]. In [54–56], a method based on solving the inverse Langevin problem for an underdamped system was proposed. This method has shown good results when measuring the interparticle interaction forces in a quasi-two-dimensional monolayer of microparticles suspended in a radio-frequency (rf) produced plasma sheath [54,61–64]. However, this method is extremely sensitive to experimental errors in determining the successive positions of particles in space, which are used to calculate particle accelerations [61]. In [57,58], a method based on the determination of natural frequencies using a system of equations for two linearly coupled oscillators was proposed. However, this method does not take into account the dissipative and random processes operating in the system, which can lead to significant errors in determining the characteristic frequencies even in underdamped systems with nonreciprocal interaction [59]. In [59,60], a correlational approach to study the nonreciprocal effective interactions between Brownian dust particles in a plasma was proposed. That approach takes into account dissipative and random processes, but may give incorrect results for systems whose spectra have any processing artifacts or spurious modes. In [65], the effect of nonreciprocal wake interaction on the vibrational spectra of a pair of microparticles in an rf produced plasma sheath was noted. Recently, nonreciprocal effective forces acting between a vertically aligned particle pair in an rf produced plasma sheath [17] and in a stratified glow DC discharge [66]

have been studied in detail. For this, the spectral response of the system to the stochastic processes occurring in it was analyzed. In this paper, we present in depth the theoretical foundations of the method used in Refs. [17,66].

Previously, analytical expressions for the vibrational spectra of confined Brownian particles (particles with thermal noise) were considered only for special cases: (1) for two particles of the same size with different types of interparticle interaction [67–71]; (2) for small-sized chain structures and quasi-two-dimensional clusters consisting of identical particles with symmetric interaction [69–71].

Here we present the general equations for the vibrational spectra of confined Brownian particles with nonreciprocal effective interactions (Sec. II). The inequality of particles in size and mass is taken into account, as well as the inhomogeneity of the external force field and heat sources responsible for Brownian motion of particles. In Sec. III, a nonperturbative inverse problem method based on spectral response to stochastic processes (SRSP) is proposed to determine interparticle and external forces acting in a multiparticle system. The following sections of the paper focus on a pair of nonreciprocally interacting particles. Section IV is devoted to the numerical simulation of the dynamics of the particle pair used to verify the SRSP method. Section V presents a detailed analysis of the spectral densities of a two-particle system and a comparison of the effectiveness of various nonperturbative methods for determining the nonreciprocal effective interparticle interaction.

II. VIBRATIONAL SPECTRA OF CONFINED PARTICLES WITH NONRECIPROCAL EFFECTIVE INTERACTIONS UNDER THE INFLUENCE OF STOCHASTIC PROCESSES

A. Basic equations

Consider a stationary system consisting of N strongly coupled particles with masses m_i and charges q_i, which are acted upon in the direction γ ($\gamma = X$, Y, or Z) by external force $F^{(\gamma)}_{\text{ext},i}$; interparticle interaction force $F^{(\gamma)}_{ji}$ acting from the jth particle on the ith one; friction force with friction coefficients ν_i and Langevin force $F^{(\gamma)}_{\text{ran},i}$, which is a source of stochastic kinetic energy for particles. Assuming that the displacement of particles $\xi^{(\gamma)}_i$ from their equilibrium position under the action of a random force $F^{(\gamma)}_{\text{ran},i}$ is limited by small deviations, we can obtain a linearization for forces in the chosen direction for each of the degrees of freedom:

$$F^{(\gamma)}_{ji} = \left\langle F^{(\gamma)}_{ji}\right\rangle + \left(\xi^{(\gamma)}_i - \xi^{(\gamma)}_j\right)\left(\frac{\partial F^{(\gamma)}_{ji}}{\partial \xi}\right) = \left\langle F^{(\gamma)}_{ji}\right\rangle + \left(\xi^{(\gamma)}_i - \xi^{(\gamma)}_j\right) m_i f^{(\gamma)}_{ji}, \tag{1}$$

$$F^{(\gamma)}_{\text{ext},i} = \left\langle F^{(\gamma)}_{\text{ext},i}\right\rangle + \xi^{(\gamma)}_i\left(\frac{\partial F^{(\gamma)}_{\text{ext},i}}{\partial \xi}\right) = \left\langle F^{(\gamma)}_{\text{ext},i}\right\rangle + \xi^{(\gamma)}_i m_i f^{(\gamma)}_i, \tag{2}$$

where the angle brackets $\langle\cdots\rangle$ denote time averaging; $f^{(\gamma)}_{ji}$ and $f^{(\gamma)}_i$ are the derivatives of the specific interparticle and external forces, that is, the stiffnesses of these specific forces. Thus, we obtain a system of equations for particle displacements $\xi^{(\gamma)}_i$:

$$\frac{d^2\xi^{(\gamma)}_i}{dt^2} = -\nu_i\frac{d\xi^{(\gamma)}_i}{dt} + \left(\sum_{j=1,j\neq i}^{N} f^{(\gamma)}_{ji} - f^{(\gamma)}_i\right)\xi^{(\gamma)}_i - \sum_{j=1,j\neq i}^{N} f^{(\gamma)}_{ji}\xi^{(\gamma)}_j + \frac{F^{(\gamma)}_{\text{ran},i}}{m_i}. \tag{3}$$

The particle displacement $\xi^{(\gamma)}_i$ is the system's response to the stochastic (random) process $F^{(\gamma)}_{\text{ran},i}$. The spectral density $S^{(\gamma)}_{\xi_i}$ of the random process $F^{(\gamma)}_{\text{ran},i}$ is the Fourier cosine transform for the corresponding autocorrelation function [72]. If $F^{(\gamma)}_{\text{ran},i}$ satisfies the conditions for delta-correlated Gaussian white noise:

$$\left\langle F^{(\gamma)}_{\text{ran},i}(t)\right\rangle = 0,\ \frac{\left\langle F^{(\gamma)}_{\text{ran},i}(t)F^{(\gamma)}_{\text{ran},i}(t+\tau)\right\rangle}{m_i^2} = S^{(\gamma)}_{\xi_i}\delta(\tau), \tag{4}$$

then the spectral densities are $S^{(\gamma)}_{\xi_i} = 2\nu_i T^{(\gamma)}_i/m_i$, where $T^{(\gamma)}_i$ is the temperature of the heat source for the particles. In this case, the spectral density of the random process at the output of the linear system is equal to the spectral density of the random process at the input of the system, multiplied by the squared modulus of the frequency transfer function of this system [73]. Then the spectral response of the system to the stochastic processes acting on it reads

$$G^{(\gamma)}_{\xi_i}(\omega) = \sum_{j=1}^{N}\frac{2\nu_j T^{(\gamma)}_j}{m_j}\bar{M}^{(\gamma)}_{\xi_i}(j), \tag{5}$$

where ω is the angular frequency of vibrations and $\bar{M}^{(\gamma)}_{\xi_i}(j)$ are the squared modules of the frequency transfer functions for Eq. (3). The complete expressions for $\bar{M}^{(\gamma)}_{\xi_i}(j)$ are presented in Appendix A, which also provides a complete description of the spectral density of the generalized linear system of coupled oscillators. Using a similar approach to extract more information about the system, it is easy to obtain the spectral densities of combined ($\sum_{j=1}^{N}\xi_j$) and relative ($\xi_i - \xi_{i+1}$) particle deviations; see Appendix C.

At the end of the section, we note that the spectral densities $G^{(\gamma)}_{V_i}$ of velocities $V^{(\gamma)}_i = d\xi^{(\gamma)}_i/dt$ are related to the spectra of the corresponding displacements by a simple relationship [72]:

$$G^{(\gamma)}_{V_i}(\omega) = \omega^2 G^{(\gamma)}_{\xi_i}(\omega). \tag{6}$$

B. Two-particle system

The vibrational spectral densities of each of the particles in the two-particle system take the form (for brevity, the indices

"1" and "2" denote oscillations ξ_1 and ξ_2, respectively):

$$G_1^{(\gamma)}(\omega) = \frac{\frac{2\nu_1 T_1^{(\gamma)}}{m_1}\left[\left(\omega^2 - f_2^{(\gamma)} + f_{12}^{(\gamma)}\right)^2 + \nu_2^2\omega^2\right] + \frac{2\nu_2 T_2^{(\gamma)}}{m_2}\left(f_{21}^{(\gamma)}\right)^2}{W^{(\gamma)}}, \tag{7a}$$

$$G_2^{(\gamma)}(\omega) = \frac{\frac{2\nu_2 T_2^{(\gamma)}}{m_2}\left[\left(\omega^2 - f_1^{(\gamma)} + f_{21}^{(\gamma)}\right)^2 + \nu_1^2\omega^2\right] + \frac{2\nu_1 T_1^{(\gamma)}}{m_1}\left(f_{12}^{(\gamma)}\right)^2}{W^{(\gamma)}}. \tag{7b}$$

In addition to the vibrations of each particle, we consider their combined and relative vibrations [the indices "+" and "−" mean combined $(\xi_1 + \xi_2)$ and relative $(\xi_1 - \xi_2)$ oscillations]:

$$G_+^{(\gamma)}(\omega) = \frac{\frac{2\nu_1 T_1^{(\gamma)}}{m_1}\left[\left(\omega^2 - f_2^{(\gamma)} + 2f_{12}^{(\gamma)}\right)^2 + \nu_2^2\omega^2\right] + \frac{2\nu_2 T_2^{(\gamma)}}{m_2}\left[\left(\omega^2 - f_1^{(\gamma)} + 2f_{21}^{(\gamma)}\right)^2 + \nu_1^2\omega^2\right]}{W^{(\gamma)}}, \tag{8}$$

$$G_-^{(\gamma)}(\omega) = \frac{\frac{2\nu_1 T_1^{(\gamma)}}{m_1}\left[\left(\omega^2 - f_2^{(\gamma)}\right)^2 + \nu_2^2\omega^2\right] + \frac{2\nu_2 T_2^{(\gamma)}}{m_2}\left[\left(\omega^2 - f_1^{(\gamma)}\right)^2 + \nu_1^2\omega^2\right]}{W^{(\gamma)}}. \tag{9}$$

The denominator in formulas (7)–(9) reads

$$W^{(\gamma)} = \left[\omega^2\left(\omega^2 - \nu_1\nu_2 - f_1^{(\gamma)} - f_2^{(\gamma)} + f_{21}^{(\gamma)} + f_{12}^{(\gamma)}\right) + f_1^{(\gamma)}f_2^{(\gamma)} - f_1^{(\gamma)}f_{12}^{(\gamma)} - f_2^{(\gamma)}f_{21}^{(\gamma)}\right]^2 + \omega^2\left[\nu_1\omega^2 + \nu_2\omega^2 + \nu_2\left(f_{21}^{(\gamma)} - f_1^{(\gamma)}\right) + \nu_1\left(f_{12}^{(\gamma)} - f_2^{(\gamma)}\right)\right]^2. \tag{10}$$

Note that combined oscillations (+) are oscillations of the center of mass with a double amplitude in the case of equal particle masses.

If the particles have the same friction coefficients ($\nu_1 = \nu_2 = \nu$), then expression (10) is simplified:

$$W^{(\gamma)} = \left\{\omega^4 + \left[\nu^2 - 2\left(\omega_1^{(\gamma)}\right)^2\right]\omega^2 + \left(\omega_1^{(\gamma)}\right)^4\right\}\left\{\omega^4 + \left[\nu^2 - 2\left(\omega_2^{(\gamma)}\right)^2\right]\omega^2 + \left(\omega_2^{(\gamma)}\right)^4\right\}, \tag{11}$$

where $\omega_i^{(\gamma)}$ are the main frequencies of the system, determined by the following expressions:

$$\left(\omega_{1(2)}^{(\gamma)}\right)^2 = \frac{f_1^{(\gamma)} + f_2^{(\gamma)} - f_{21}^{(\gamma)} - f_{12}^{(\gamma)} \mp \sqrt{\left(f_1^{(\gamma)} - f_2^{(\gamma)} - f_{21}^{(\gamma)} + f_{12}^{(\gamma)}\right)^2 + 4f_{21}^{(\gamma)}f_{12}^{(\gamma)}}}{2}. \tag{12}$$

If the particles have the same friction coefficients ($\nu_1 = \nu_2 = \nu$), symmetrical interaction ($f_{21}^{(\gamma)} = f_{12}^{(\gamma)} = f_{\text{int}}^{(\gamma)}$), and equal noise intensities ($\frac{2\nu_1 T_1^{(\gamma)}}{m_1} = \frac{2\nu_2 T_2^{(\gamma)}}{m_2} = S^{(\gamma)}$), then the spectral densities of the particles are transformed:

$$G_{1(2)}^{(\gamma)}(\omega) = \frac{A_{1(2)}^{(\gamma)}}{\omega^4 + \left[\nu^2 - 2\left(\omega_1^{(\gamma)}\right)^2\right]\omega^2 + \left(\omega_1^{(\gamma)}\right)^4} + \frac{A_{2(1)}^{(\gamma)}}{\omega^4 + \left[\nu^2 - 2\left(\omega_2^{(\gamma)}\right)^2\right]\omega^2 + \left(\omega_2^{(\gamma)}\right)^4}, \tag{13}$$

where

$$A_1^{(\gamma)} = \frac{S^{(\gamma)}}{2}\left(1 - \frac{f_1^{(\gamma)} - f_2^{(\gamma)}}{D^{(\gamma)}}\right), \quad A_2^{(\gamma)} = \frac{S^{(\gamma)}}{2}\left(1 + \frac{f_1^{(\gamma)} - f_2^{(\gamma)}}{D^{(\gamma)}}\right), \quad D^{(\gamma)} = \sqrt{\left(f_1^{(\gamma)} - f_2^{(\gamma)} - f_{21}^{(\gamma)} + f_{12}^{(\gamma)}\right)^2 + 4f_{21}^{(\gamma)}f_{12}^{(\gamma)}}.$$

Thus, the spectral density of particle displacements is a superposition of the spectral densities of two classical damped oscillators [72].

If the particles also have the same friction coefficients ($\nu_1 = \nu_2 = \nu$), symmetric interaction ($f_{21}^{(\gamma)} = f_{12}^{(\gamma)} = f_{\text{int}}^{(\gamma)}$), and equal stiffnesses of the specific external force ($f_1^{(\gamma)} = f_1^{(\gamma)} = f_{\text{ext}}^{(\gamma)}$), then the expressions for combined and relative oscillations of particles (8) and (9) take the form of the spectral density of the classical oscillator:

$$G_{+(-)}^{(\gamma)}(\omega) = \frac{2\nu\left(\frac{T_1^{(\gamma)}}{m_1} + \frac{T_2^{(\gamma)}}{m_2}\right)}{\omega^4 + \left[\nu^2 - 2\left(\omega_{+(-)}^{(\gamma)}\right)^2\right]\omega^2 + \left(\omega_{+(-)}^{(\gamma)}\right)^4}, \tag{14}$$

where frequencies $\omega_{+(-)}^{(\gamma)}$ are a special case of formula (12):

$$\left(\omega_+^{(\gamma)}\right)^2 = f_{\text{ext}}^{(\gamma)}, \tag{15}$$

$$\left(\omega_-^{(\gamma)}\right)^2 = f_{\text{ext}}^{(\gamma)} - 2f_{\text{int}}^{(\gamma)}. \tag{16}$$

III. INVERSE PROBLEM (METHOD)

Applying the Fourier transform to the trajectories of strongly coupled Brownian particles obtained in the experiment, we get the spectral densities of particle oscillations, as well as the spectral densities of combined and relative oscillations ($\tilde{G}_1^{(\gamma)}$, $\tilde{G}_2^{(\gamma)}$, $\tilde{G}_+^{(\gamma)}$, and $\tilde{G}_-^{(\gamma)}$ in the case of two particles). Here and below, the upper tilde means that the value was measured in a numerical or laboratory experiment (in this

work we will focus on the analysis of numerical results). By approximating the spectral densities measured in the experiment with the analytical formulas obtained in the previous section, it is possible to determine not only the stiffnesses $f_{ji}^{(\gamma)}$ of the specific interaction forces, but also the stiffnesses $f_i^{(\gamma)}$ of the specific external forces acting on the particles in equilibrium positions, as well as the friction coefficients of particles in the medium ν_i and parameters $T_i^{(\gamma)}/m_i$. For example, the approximation can be carried out by minimizing the absolute residual with additional coefficients,

$$\rho = \sum_n \varsigma_n^2 \sum_j \left[\tilde{G}_n^{(\gamma)}(\tilde{\omega}_j) - G_n^{(\gamma)}(\tilde{\omega}_j)\right]^2, \qquad (17)$$

using the simplex search method of Lagarias *et al.* [74], where $\varsigma_n = \max_{m,j} \tilde{G}_m^{(\gamma)}(\tilde{\omega}_j)/\max_j \tilde{G}_n^{(\gamma)}(\tilde{\omega}_j)$, and summation is performed over all discrete frequencies $\tilde{\omega}_j$, as well as over all available spectra (i.e., for $n = 1, 2, +, -$ in the case of two particles). Additional coefficients ς_n, which are the ratio of the maximum oscillation amplitude among all spectra to the maximum in the nth spectrum, allow us to take into account the difference in the amplitudes $\tilde{G}_n^{(\gamma)}$, since they can differ by several orders of magnitude. Also, the operation of the method is possible using the spectral densities of velocities obtained both by direct calculation and by formal transformation of the particle displacement spectra taking into account (6). Note that only one spectrum is sufficient for the successful application of the method; however, the accuracy of determining the desired parameters will be noticeably lower, and using the combined and relative displacement spectra makes it possible to avoid incorrect sets of parameters [17]. We also note that spectral densities were previously found for various combinations of particle displacements in many-particle systems [69–71], which make it possible to obtain the spectra of isolated harmonics of chain and quasi-two-dimensional systems with up to seven particles interacting with a symmetric potential. However, complex combinations of displacements instead of combined and relative displacements give almost identical results for solving the inverse problem; moreover, the use of combined and relative displacements is a more universal approach, especially in the case of systems with a large number of particles.

Also important are the data discreteness requirements for constructing the spectral density. Note that, according to the Nyquist-Shannon sampling theorem [75], the maximum frequency value for the spectral density $\omega_{\max}$ obtained as a result of the discrete Fourier transform is determined by the experimental data recording step Δt: $\omega_{\max} = \pi/\Delta t$. The spectral step is determined by the duration of the transformed fragment of the experiment recording $\Delta\omega = \pi/N\Delta t = \omega_{\max}/N$, where N is the number of analyzed time points (for example, the number of frames on a video fragment of the experiment). Thus, it is necessary to fulfill the condition $\omega_w \gg \Delta\omega$ (ω_w is the full width at half maximum of spectral peaks); i.e., a sufficient duration of the converted fragment is necessary to avoid a distortion of the shape of the spectra [76,77]. However, a decrease in $\Delta\omega$ leads to signal noise and it is necessary to use averaging of the spectra obtained for different fragments of particle trajectories to improve the accuracy of the method. We also note that for the two-particle system the condition $\omega_{\max} \gg \max(\omega_1^{(\gamma)}, \omega_2^{(\gamma)})$ must be met, i.e., a sufficient frame rate of the video camera used in the experiment is required.

IV. NUMERICAL SIMULATION (VALIDATION)

The obtained analytical expressions for the spectral densities and technique described in Sec. III were tested on the results of numerical simulation in a wide range of parameters. The numerical simulation of stochastic processes was carried out by the Langevin molecular dynamics method. The procedure is described in detail in Refs. [78–81].

The analytical expressions and the solution to the inverse problem presented in the previous sections apply to many-particle systems. Next, the analysis will focus on a pair of particles with vertical alignment (relative to gravity), simulating a system of dust particles in a gas-discharge plasma. Vertical alignment was chosen because the nonreciprocity effect is pronounced in this configuration [65,66].

A vertical pair consisting of generally nonidentical particles with masses m_i, charges q_i, friction coefficients ν_i, and temperatures T_i, corresponding to the intensities of random processes acting on the particles (Langevin thermostats), was simulated. The case of identical particles ($m_i = m_0$, $q_i = q_0$, $\nu_i = \nu_0$, $T_i = T_0$) was also considered. The particles were in the gravity field compensated by the electric field $\mathbf{E}$ of a linear trap with circular symmetry in the horizontal plane with radial components $E^{(X)} = \alpha x$, $E^{(Y)} = \alpha y$ and vertical component $E^{(Z)} = E_0 + \beta z$. Here x, y, z are the coordinates along the corresponding axes (the Z axis is directed antiparallel to gravity), α and β are the magnitudes of the electric field gradients, and the value of E_0 is determined by the balance of forces acting in the system. In accordance with the field gradients, the characteristic frequencies of the trap $\omega_t^{(X)} \equiv \omega_t^{(Y)} = \sqrt{\alpha q_0/m_0}$ in the transverse plane and $\omega_t^{(Z)} = \sqrt{\beta q_0/m_0}$ in the longitudinal. If the ith particle has m_0 and q_0, then $f_i^{(\gamma)} = (\omega_t^{(\gamma)})^2$. The following model parameters were set: $\alpha/\beta = 4$, $\omega_t^{(Z)} = 10\ \mathrm{s}^{-1}$, $\omega_t^{(X)} = 20\ \mathrm{s}^{-1}$, $m_0 = 10^{-10}$ g, $q_0 = -0.5\beta\Delta r^3 = -4658e$ ($\Delta r = 0.1$ cm is the average distance between particles; e is the elementary electric charge), $T_0 = q_0^2/150\Delta r \approx 0.21$ eV. The selected model parameters are typical for laboratory experiments with dusty plasmas [17,61–63,66,82,83]. Note that under laboratory conditions the temperature T_0 can be higher than the temperature of the buffer gas [17,84].

Typically, numerical simulations of the dynamics of dust particles in a gas-discharge plasma are performed for the particles interacting via the point-wake model potential, which is often used for a qualitative description of wake-mediated forces generated by the flow of ions past charged particles in plasma [6,7,60]. When a microparticle is immersed in a low-pressure gas discharge, it acquires a significant negative charge (typically, up to 10^3–10^4 elementary charges) and creates an ion wake due to the flow of ions passing by the particle in the direction of the local electric field [44,45]. In the point-wake model, a virtual oppositely charged particle is rigidly bound to the real particle and affects only the neighboring real particle, while the latter has no effect on the virtual one. However, due to the peculiarities of the point-wake model, the resulting particle system can be unstable, and this does

not allow calculations to be carried out in a wide range of parameters.

For simplicity and convenience, the nonreciprocity of the interaction was modeled using the modified Coulomb interaction:

$$\mathbf{F}_{ji} = \epsilon_i q_i q_j \frac{\mathbf{r}_i - \mathbf{r}_j}{|\mathbf{r}_i - \mathbf{r}_j|^3}, \tag{18}$$

where $\mathbf{r}_i$ is the radius vector of the ith particle, $\epsilon_{1,2} = 1 \mp R$, and R is the dimensionless nonreciprocity parameter characterizing the magnitude of the symmetry breaking of the interaction between particles ($R = |\langle \mathbf{F}_{21} \rangle + \langle \mathbf{F}_{12} \rangle| / |\langle \mathbf{F}_{21} \rangle - \langle \mathbf{F}_{12} \rangle|$) [6,9]. This potential is convenient for modeling, since it allows one to control the nonreciprocity when other parameters (in particular, the interparticle distance) are fixed. In the case of equality of the stiffnesses of the specific external forces [$f_1^{(\gamma)} = f_2^{(\gamma)}$; i.e., $\omega_2^{(\gamma)} \equiv \omega_+^{(\gamma)}$ according to formula (12)] and using (18), the variation of R preserves such a relationship between the interaction forces that the frequency value $\omega_1^{(\gamma)}$ (12) does not depend on R; that is, $\omega_1^{(\gamma)} \equiv \omega_-^{(\gamma)}$. Thus, the stiffnesses of the specific interaction forces have the following values: $f_{ji}^{(X)} = \frac{F_{ji}(\Delta r)}{m_j \Delta r} = \epsilon_i \frac{q_i q_j}{m_i \Delta r^3}$, $f_{ji}^{(Z)} = \frac{F'_{ji}(\Delta r)}{m_i} = -2\epsilon_i \frac{q_i q_j}{m_i \Delta r^3}$. In the case of identical particles with $R = 0$, it turns out that $f_{\text{ext}}^{(X)} = 400\ \text{s}^{-2}$, $f_{\text{int}}^{(X)} = 50\ \text{s}^{-2}$, $f_{\text{ext}}^{(Z)} = 100\ \text{s}^{-2}$, $f_{\text{int}}^{(Z)} = -100\ \text{s}^{-2}$, for external and interparticle forces.

When modeling, the integration step ranged from $\Delta t = (40 \max[\omega_t^{(\gamma)}; \nu_i])^{-1}$ to $(80 \max[\omega_t^{(\gamma)}; \nu_i])^{-1}$, that is, from 1/800 to 1/8000 s, depending on the conditions of the problem. The recording of particle trajectories was performed after reaching equilibrium in the system. The value of the ratio $\varrho = \nu/\omega_t^{(\gamma)}$ varied from 0.005 to 10. In all considered cases, a vertical configuration of particles was observed and the simulated systems were stable. The particle velocity distribution functions corresponded to the Maxwell distribution.

The spectral density calculations were carried out for particle trajectories $x(t)$, $y(t)$, and $z(t)$ using the fast Fourier transform procedure in the MATLAB application package.

In a physical experiment, the finite spatial resolution of the video camera, peculiarities of the procedure for recognizing the particle image, and determining its center of mass lead to an error in measuring the particle position in space. To simulate the measurement errors, the obtained particle trajectories were distorted as follows:

$$\check{\mathbf{r}}_i = \mathbf{r}_i + N(0, p) \tag{19}$$

where $N(0, p)$ is a random number from the normal distribution with zero mean and standard deviation parameter $p \approx 10^{-3}$ cm $p/\Delta r \approx 10^{-2}$, which is the usual pixel size in cameras used in real experiments.

V. RESULTS AND DISCUSSION

A. Influence of system parameters on the vibrational spectral densities

1. Influence of nonreciprocity

Figures 1(a) and 1(b) show vibrational spectral densities in a system of two particles with different nonreciprocity parameters R; Fig. 1(c) shows a schematic representation of a simulated pair of particles in an electrostatic trap in the presence of gravity. The presented spectral densities are normalized as follows: $\tilde{G}_i^{*(\gamma)} = n^{(\gamma)} \tilde{G}_i^{(\gamma)}$, where $n^{(\gamma)} = (\nu \omega_t^{(\gamma)})^2 / S^{(\gamma)} = m_0 \nu (\omega_t^{(\gamma)})^2 / 2T_0$. The notation $i = 1$ corresponds to the lower particle experiencing a change in the nature of the action (effective attraction) with increasing R. First of all, we note that the interaction model (18) gives qualitatively similar results to the spectra obtained in experiments [17,65,66]. Let us consider the general patterns: the mutual arrangement of the peaks corresponding to the frequencies $\omega_+^{(\gamma)}$ and $\omega_-^{(\gamma)}$ differs along the axes. This distinction is explained by Eq. (16): in the case of $f_{\text{int}}^{(\gamma)} > 0$, the peak $\omega_-^{(\gamma)}$ is closer to zero than $\omega_+^{(\gamma)}$, which is observed along the X axis, and vice versa. The value of $f_{\text{int}}^{(\gamma)}$ determines the distance between the peaks, and since $|f_{\text{int}}^{(Z)}/f_{\text{ext}}^{(Z)}| > |f_{\text{int}}^{(X)}/f_{\text{ext}}^{(X)}|$, so the peaks are located closer along the X axis, which complicates the visual selection of peaks, especially with increasing R.

With an increase in the nonreciprocity, the amplitudes of oscillations and, accordingly, the kinetic energy of particles increase due to the work of nonreciprocal effective interparticle forces [1,6,85]. In particular, for the results presented in Figs. 1(a) and 1(b), the ratio of the average kinetic energy of two particles to the Langevin thermostat temperature: $2E_{R=0.2}/T_0 \approx 1.03$, $2E_{R\approx1}/T_0 \approx 1.6$, $2E_{R=2}/T_0 \approx 3.3$. At the same time, the distribution of the pumped energy is nonuniform over the degrees of freedom, as well as between the particles, for example, $2E_{1,R=2}^{(Z)}/T_0 \approx 2.7$, $2E_{2,R=2}^{(Z)}/T_0 \approx 6.1$, which is in accordance with the previously obtained relations [7,69,86,87]. Such an uneven distribution of energy is a typical situation for active systems [88], including those with nonreciprocal interactions. Note that the expressions for the spectral density, for example, (5), (7)–(9), and (13) and (14), include precisely the temperatures of heat sources (preset temperatures), and not the steady-state effective kinetic temperatures of the particles.

Let us consider the individual spectra. The spectral density of relative displacements $\tilde{G}_-^{(\gamma)}$ is a single peak at any R for the interaction models used in this study, and for model (18) $\tilde{G}_-^{(\gamma)}$ remains unchanged; see Figs. 1(a) and 1(b). On the spectrum $\tilde{G}_+^{(\gamma)}$, the appearance and further growth of the second peak corresponding to $\omega_-^{(\gamma)}$ is observed with increasing R, which is a clear manifestation of nonreciprocity. It should be noted that the difference in the derivatives of the specific external forces ($f_1^{(\gamma)} \neq f_2^{(\gamma)}$) can also be manifested by the appearance of a peak $\omega_-^{(\gamma)}$ in the spectrum of the combined particle displacements; therefore, a sufficient condition for the presence of nonreciprocity is the simultaneous presence of the peak $\omega_-^{(\gamma)}$ in the spectrum of the combined displacements and the absence of $\omega_+^{(\gamma)}$ in the spectrum of the relative displacements. The absence of the peak $\omega_+^{(\gamma)}$ in the spectrum of the relative displacements is the criterion $f_1^{(\gamma)} = f_2^{(\gamma)}$. Then we consider the influence of external forces in more detail. The spectra of particles $\tilde{G}_1^{(\gamma)}$ and $\tilde{G}_2^{(\gamma)}$ contain both peaks; however, their amplitudes change nonlinearly with increasing R: a decrease in the absolute value of the force $|\mathbf{F}_{21}|$, with which the upper particle acts on the lower one, to zero (that is, a change in R from 0 to 1) is reflected by a decrease

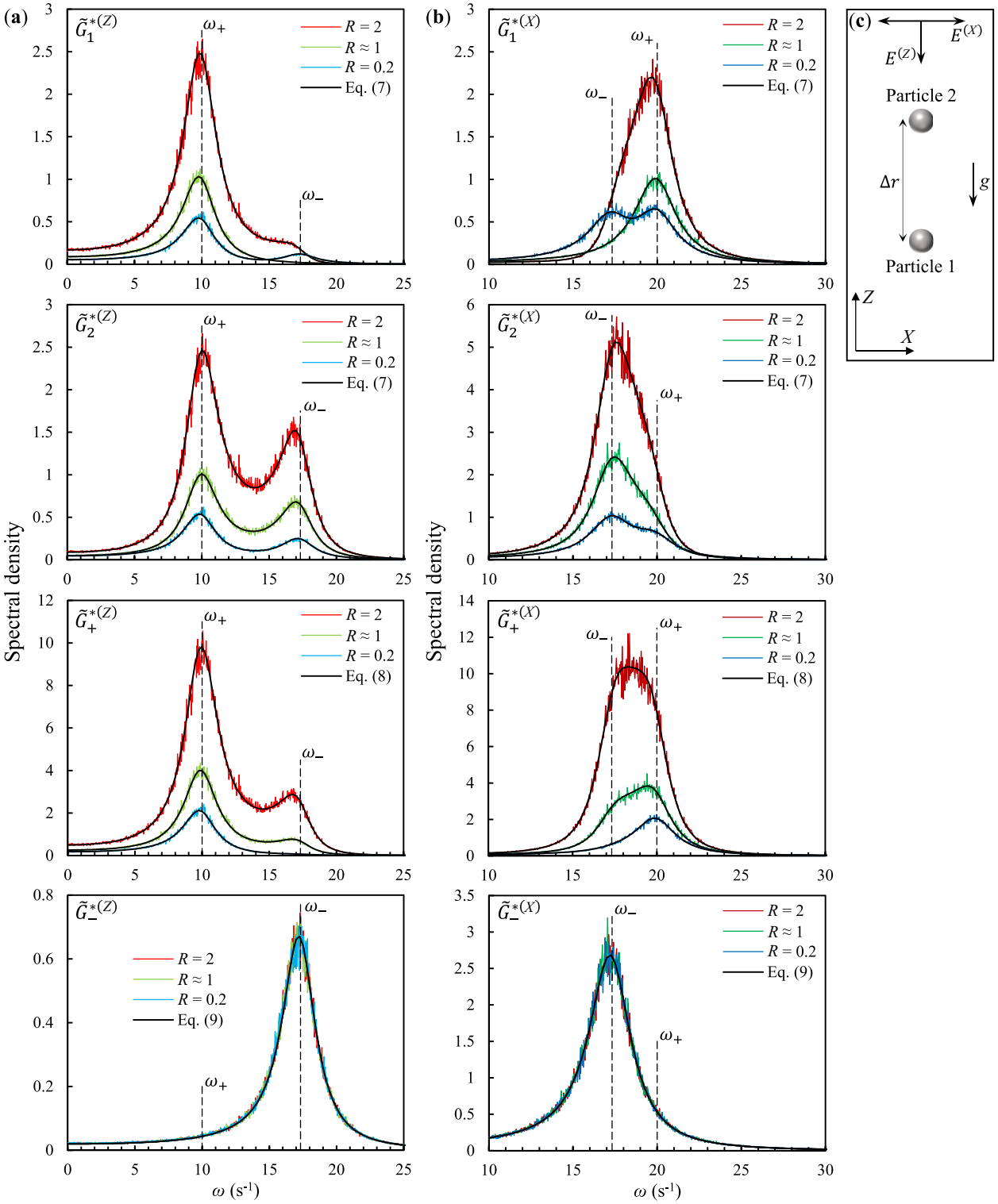

FIG. 1. Normalized spectral densities $\tilde{G}_n^{*(\gamma)}$ ($n = 1, 2, +, -$) for the friction coefficient $\nu = 3\,\mathrm{s}^{-1}$ and various values of the nonreciprocity parameter R of two particles interacting with the force (18) (a) in the vertical direction $\gamma = Z$ and (b) in the horizontal direction $\gamma = X$. The black lines show the analytical solutions (7)–(9), the colored lines show the results of numerical simulation, and the dotted lines indicate the main frequencies $\omega_+^{(\gamma)}$ (15) and $\omega_-^{(\gamma)}$ (16). (c) Schematic representation of a simulated pair of particles in an electrostatic trap in the presence of gravity.

in the peak $\omega_-^{(\gamma)}$ of the lower particle spectrum until it disappears, and vice versa: the peak $\omega_-^{(\gamma)}$ of the upper particle spectrum acquires the maximum amplitude relative to the peak $\omega_+^{(\gamma)}$. With further growth of R, reverse processes occur, since $\mathbf{F}_{21}$ changes sign (direction) and increases its absolute value.

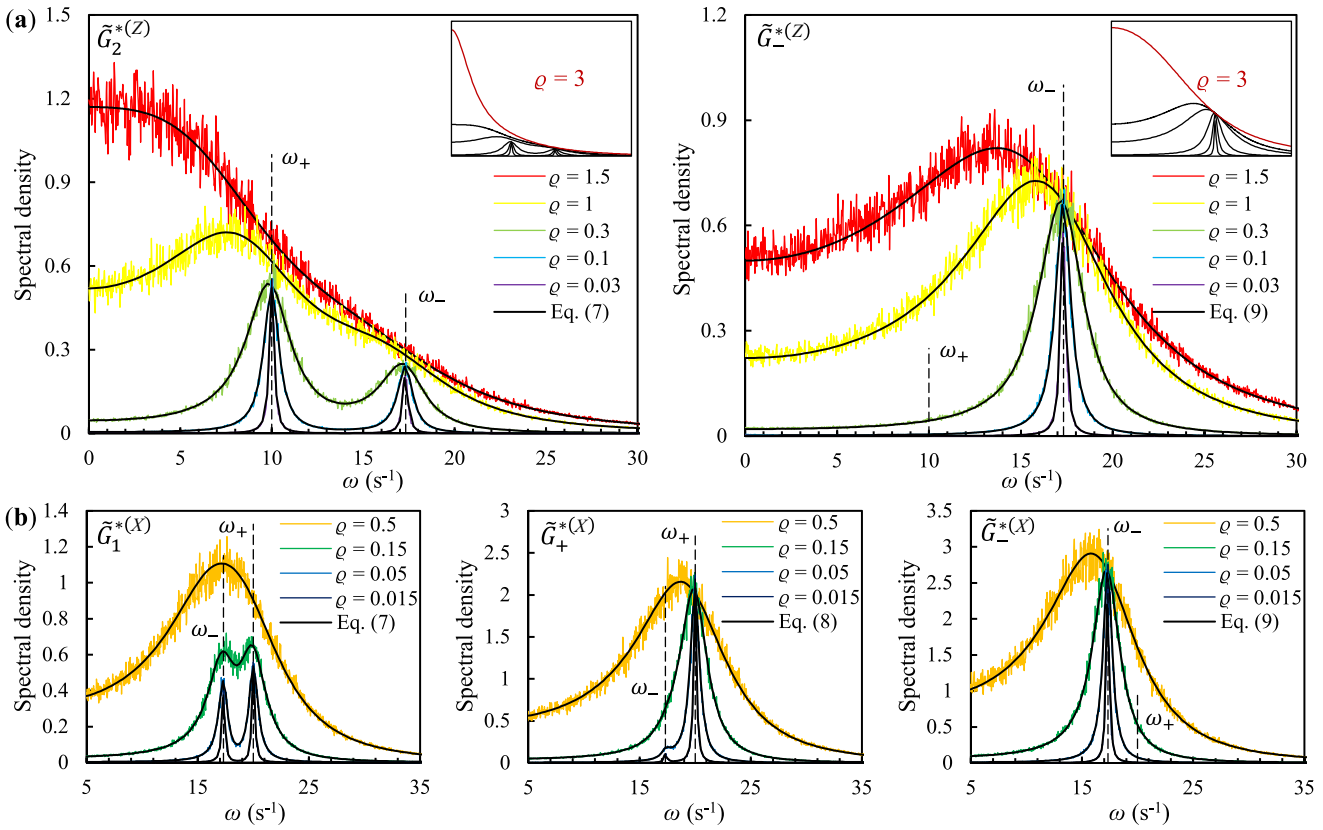

FIG. 2. Normalized spectral densities $\tilde{G}_n^{*(\gamma)}$ of the two-particle system with different values of $\varrho = \nu/\,\omega_i^{(\gamma)}$ and $R = 0.2$. (a) Displacements of the upper particle ($n = 2$) and relative displacements of particles ($n = -$) in the vertical direction $\gamma = Z$, (b) displacements of the lower particle ($n = 1$), and combined and relative displacements ($n = +,\ -$) for $\gamma = X$. Presented frictions: $\nu = 30\,\mathrm{s}^{-1}$ ($\varrho^{(Z)} = 3$), $\nu = 15\,\mathrm{s}^{-1}$ ($\varrho^{(Z)} = 1.5$), $\nu = 10\,\mathrm{s}^{-1}$ ($\varrho^{(Z)} = 2\varrho^{(X)} = 1$), $\nu = 3\,\mathrm{s}^{-1}$ ($\varrho^{(Z)} = 2\varrho^{(X)} = 0.3$), $\nu = 1\,\mathrm{s}^{-1}$ ($\varrho^{(Z)} = 2\varrho^{(X)} = 0.1$), $\nu = 0.3\,\mathrm{s}^{-1}$ ($\varrho^{(Z)} = 2\varrho^{(X)} = 0.03$). The black lines show the analytical solutions (7)–(9), the colored lines show the results of numerical simulation, and the dotted lines indicate the main frequencies $\omega_+^{(\gamma)}$ (15) and $\omega_-^{(\gamma)}$ (16); in (a) the inset also shows a schematic representation for $\varrho = 3$.

2. *Influence of dissipation*

The effect of friction on the vibrational spectral densities is shown in Fig. 2 for the displacements of the upper particle, and combined and relative displacements depending on $\varrho = \nu/\,\omega_i^{(\gamma)}$. For $\varrho \ll 1$, the spectra are pronounced peaks that are in good agreement with the analytical values (15) and (16), but as friction increases, the peaks shift towards lower frequencies [89]. As ϱ increases, the peaks also merge into a single "hump" at $\nu/\,|f_{\mathrm{int}}^{(\gamma)}/f_{\mathrm{ext}}^{(\gamma)}| > 10$, which is especially visible along the X axis due to the proximity of the peaks; a further increase in friction leads to the degeneration of the spectra to a maximum at zero for $\varrho > 1.5$, see an example in Fig. 2(a), where schematic representations are given for $\varrho = 3$. Thus, an increase in the friction value makes it difficult to analyze the spectral characteristics of systems.

However, with an increase in friction, the significance of the spectra of combined and relative vibrations increases, since in the case of merging of peaks in the spectra of particle oscillations, the spectra of sums and differences make it possible to show the peaks separately, which is especially important when they are close together, and which simplifies the analysis; see Fig. 2(b) ϱ = 0.5. A similar effect is also present with an increase in R. However, the growing peak $\omega_-^{(\gamma)}$, which is responsible for the nonreciprocity, can worsen the visual analysis of the spectrum $\tilde{G}_+^{*(\gamma)}$; see Fig. 1(b). Also in the case of oscillation spectra close to degeneracy at zero, the spectra of combined or relative vibrations can provide information about one of the peaks [69,70]. For example, if $\omega_-^{(\gamma)} > \omega_+^{(\gamma)}$, then the spectrum of the difference $\tilde{G}_-^{*(\gamma)}$ retains the form of a peak; see Fig. 2(a) $\varrho = 1.5$, and vice versa. The influence of this effect is more pronounced, the farther the peaks are from each other. However, in any case, as friction increases, the displacement spectra degenerate into a peak at zero; see the insets in Fig. 2(a). In this case, using velocity spectra instead of displacement spectra can help.

Figure 3 shows the velocity spectral densities for some cases from Fig. 2(a). The velocity spectra are normalized: $\tilde{G}_{V_i}^{*(\gamma)} = n^{(\gamma)}\tilde{G}_{V_i}^{(\gamma)}$, where $n^{(\gamma)} = \nu^2/S^{(\gamma)} = m_0\nu/2T_0$. With small friction, the velocity spectra are similar to the displacement spectra, but with increasing friction, a difference is noticeable. When the displacement spectra have already degenerated into a maximum at zero, see the inset in Fig. 2(a) ($\varrho = 3$), the spectra of combined and relative velocities retain their peak positions at unchanged frequencies; see Figs. 3(b) and 3(c). Thus, due to the additional factor ω^2 in Eq. (6), the

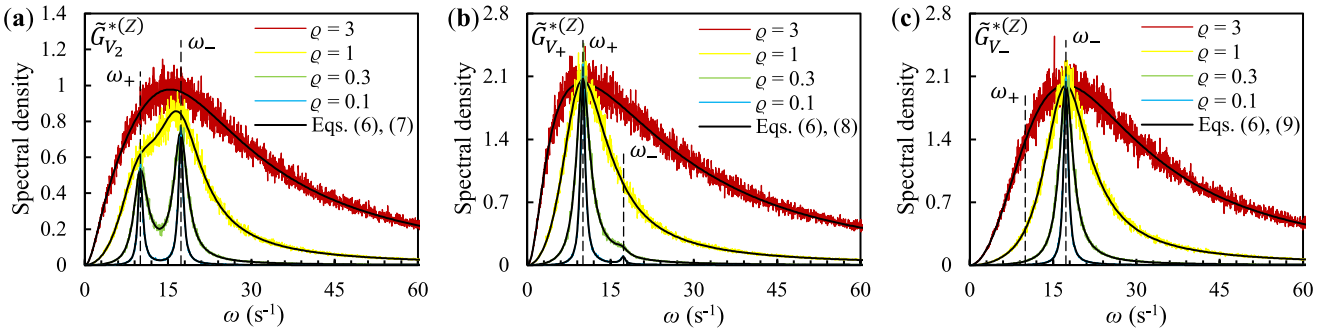

FIG. 3. Normalized spectral densities $\tilde{G}^{*(Z)}_{V_n}$ for different values of $\varrho = \nu/\,\omega_t^{(Z)}$ and $R = 0.2$. (a) Velocity of the upper particle ($n = 2$), (b) combined ($n = +$), and (c) relative velocities ($n = -$) in the vertical direction Z. Presented frictions: $\nu = 30\,\mathrm{s}^{-1}$ ($\varrho^{(Z)} = 3$), $\nu = 10\,\mathrm{s}^{-1}$ ($\varrho^{(Z)} = 1$), $\nu = 3\,\mathrm{s}^{-1}$ ($\varrho^{(Z)} = 0.3$), $\nu = 1\,\mathrm{s}^{-1}$ ($\varrho^{(Z)} = 0.1$). The black lines show the analytical solutions (7)–(9), the colored lines show the results of numerical simulation, and the dotted lines indicate the main frequencies $\omega_+^{(\gamma)}$ (15) and $\omega_-^{(\gamma)}$ (16).

velocity spectra expand the possibilities of analyzing spectral characteristics.

3. *Influence of heat sources*

Consideration of the effects associated with the difference in the particle parameters lets us begin with the difference in the magnitude of heat sources ($T_1^{(\gamma)} \neq T_2^{(\gamma)}$). Figures 4(a) and 4(b) show that the oscillation amplitudes of the particles changed insignificantly, despite the fact that the values of the preset temperatures differ for the particles by a factor of 3 and 9, respectively. This phenomenon is explained by the redistribution of average kinetic energy between particles [68,90,91] within one degree of freedom, which in the case of reciprocal interaction ($R = 0$) is expressed as follows: $2(E_1^{(\gamma)} + E_2^{(\gamma)}) = T_1^{(\gamma)} + T_2^{(\gamma)}$.

It is noteworthy that despite the larger temperature difference in Fig. 4(b) ($9T_1^{(\gamma)} = T_2^{(\gamma)} = T_0$), the kinetic energies of the particles in Fig. 4(a) ($3T_1^{(\gamma)} = T_2^{(\gamma)} = 3T_0$) differ significantly from each other: $E_2^{(Z)}/E_1^{(Z)} \approx 1.3$ and $E_2^{(X)}/E_1^{(X)} \approx 1.8$, respectively, which is reflected in the differences in the amplitudes of the spectral densities of particle oscillations. This feature is explained by the efficiency of energy redistribution, which, in the case of equality of derivatives for external ($f_1^{(\gamma)} = f_2^{(\gamma)} = f_{\mathrm{ext}}^{(\gamma)}$) and interparticle ($f_{21}^{(\gamma)} = f_{12}^{(\gamma)} = f_{\mathrm{int}}^{(\gamma)}$) forces, is determined by the value of the ratio $|f_{\mathrm{int}}^{(\gamma)}/f_{\mathrm{ext}}^{(\gamma)}|$; conditionally, the larger the value, the stronger the redistribution [68,90,91], which is observed in our case ($|f_{\mathrm{int}}^{(Z)}/f_{\mathrm{ext}}^{(Z)}| > |f_{\mathrm{int}}^{(X)}/f_{\mathrm{ext}}^{(X)}|$). Note that despite small differences in the amplitudes of particle oscillations at main frequencies in Fig. 4(b), the shape of the spectral densities is significantly different. The spectra of combined and relative displacements retain their shape, changing only the amplitude in proportion to the value of $S_1^{(\gamma)} + S_2^{(\gamma)}$ according to formula (14); see Fig. 4(c).

4. *Nonidentical particles*

Figure 5 shows the effect of different friction coefficients of particles ($\nu_1 \neq \nu_2$) on the oscillation spectra in comparison with the case of equal friction. The influence is similar to the general change in friction (see Sec. V A 2), when the peaks merge into one and subsequently degenerate into a maximum at zero with increasing friction, see Fig. 5(a), and pronounced peaks appear with decreasing friction; see Fig. 5(b). Note that the changes are most pronounced in the spectrum of the particle with a modified friction coefficient. In this case, the spectra of combined and relative displacements undergo

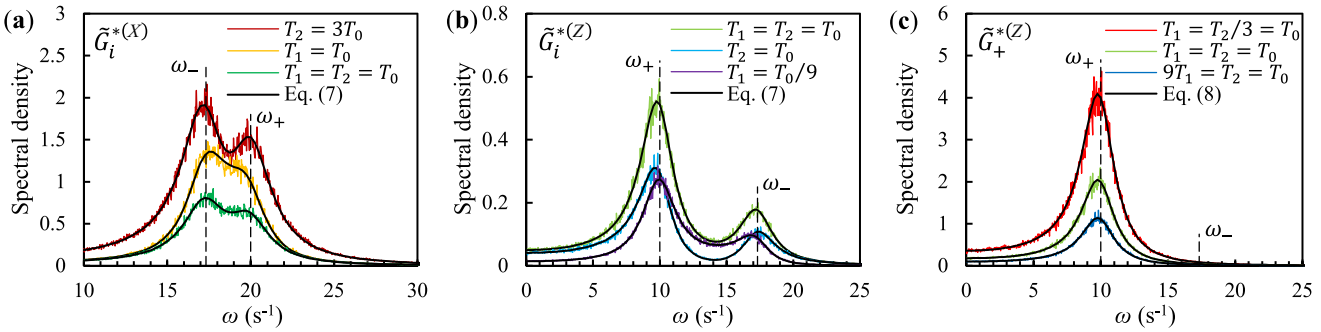

FIG. 4. Normalized spectral densities $\tilde{G}_i^{*(\gamma)}$ ($i = 1, 2$) and $\tilde{G}_+^{*(\gamma)}$ for particles with $R = 0$, $\nu = 3\,\mathrm{s}^{-1}$, and different Langevin thermostat temperatures ($T_1^{(\gamma)} \neq T_2^{(\gamma)}$): (a) $T_1^{(\gamma)} = T_0$, $T_2^{(\gamma)} = 3T_0$, $\gamma = X$; (b) $T_1^{(\gamma)} = T_0/9$, $T_2^{(\gamma)} = T_0$, $\gamma = Z$; (c) the previously given temperature ratios in the case of combined displacements of particles at $\gamma = X$. For comparison the case of $\tilde{G}_1^{*(\gamma)} \equiv \tilde{G}_2^{*(\gamma)}$ and $\tilde{G}_+^{*(\gamma)}$ at $T_1^{(\gamma)} = T_2^{(\gamma)} = T_0$ is also shown. The black lines show the analytical solutions (7) and (8); the colored lines show the results of numerical simulation, the dotted lines indicate the main frequencies $\omega_+^{(\gamma)}$ (15) and $\omega_-^{(\gamma)}$ (16).

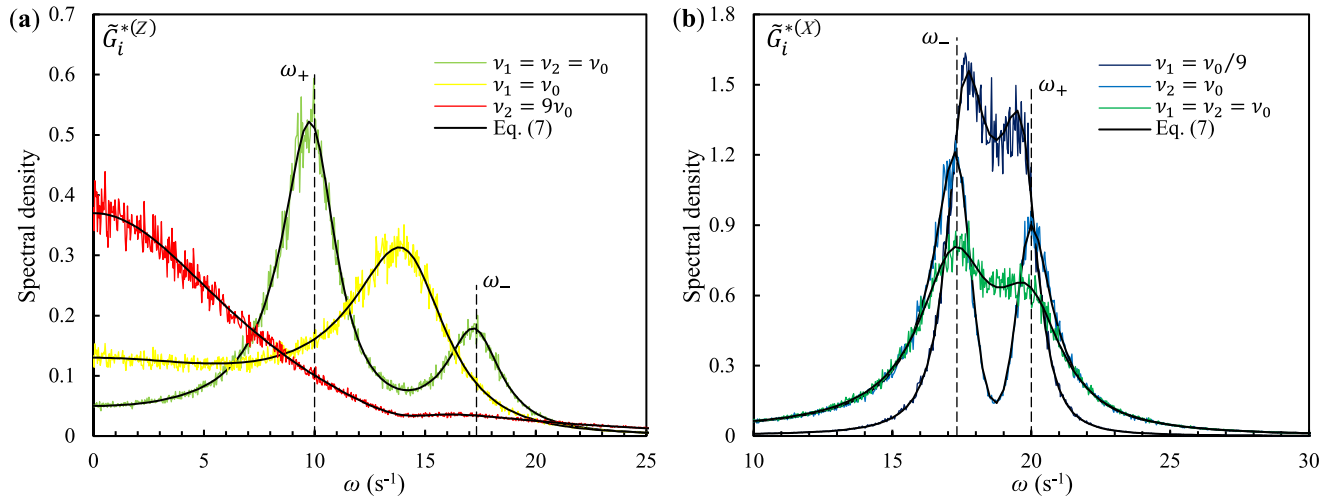

FIG. 5. Normalized spectral densities $\tilde{G}_i^{*(\gamma)}$ $(i = 1, 2)$ for particles with $R = 0$ and different friction coefficients ($\nu_1 \neq \nu_2$). (a) $\nu_1 = \nu_0$, $\nu_2 = 9\nu_0$, $\gamma = Z$; (b) $\nu_1 = \nu_0$, $\nu_2 = \nu_0/9$, $\gamma = X$, where $\nu_0 = 3\,\mathrm{s}^{-1}$. For comparison the case of $\tilde{G}_1^{*(\gamma)} \equiv \tilde{G}_2^{*(\gamma)}$ for $\nu_1 = \nu_2 = \nu_0$ is also shown. The black lines show the analytical solutions (7), the colored lines show the results of numerical simulation, and the dotted lines indicate the main frequencies $\omega_+^{(\gamma)}$ (15) and $\omega_-^{(\gamma)}$ (16).

insignificant changes: peaks thicken with a decrease in their amplitude with increasing friction, and vice versa.

Figure 6 shows the effect of different particle sizes ($a_1 \neq a_2$), and the corresponding difference in the remaining parameters of the particles, that is, mass, charge, and friction coefficients ($m_i \sim a_i^3$, $q_i \sim a_i$, $\nu_i \sim 1/a_i$), on the spectral oscillation densities. These changes affect the stiffnesses of the specific forces acting on the particles. For particle sizes $a_1 = 4a_2 = 4a_0$ and reciprocal interaction ($R = 0$) we have $f_1^{(Z)} = f_2^{(Z)}/16 = f_{\mathrm{ext}}^{(Z)}/16$, $f_{21}^{(Z)} = f_{\mathrm{int}}^{(Z)}/40$, $f_{12}^{(Z)} = 1.6 f_{\mathrm{int}}^{(Z)}$. Such variations in stiffnesses lead to a change in the main frequencies $\omega_{1(2)}^{(\gamma)}$ in accordance with (16), in contrast to identical particles for which $\omega_1^{(\gamma)} \equiv \omega_-^{(\gamma)}$ and $\omega_2^{(\gamma)} \equiv \omega_+^{(\gamma)}$ (in Fig. 6, the frequencies have shifted closer to zero). First, we note that inequality of the stiffnesses of the specific interaction forces ($f_{21}^{(\gamma)} \neq f_{12}^{(\gamma)}$) along with the equality $f_1^{(\gamma)} = f_2^{(\gamma)}$ leads to the fact that the peaks $\omega_+^{(\gamma)}$ on the particle oscillation spectra have the same shapes and amplitudes, which can be seen in Fig. 1, while the peak $\omega_-^{(\gamma)}$ of the ith particle decreases to visual indefinability with decreasing $|f_{ji}^{(\gamma)}/f_{ij}^{(\gamma)}|$ at $|f_{ji}^{(\gamma)}/f_{ij}^{(\gamma)}| < 1$. For the jth particle, both peaks are preserved, which can be seen in Fig. 1 for the case of $R \approx 1$, and the changes in the spectra of combined and relative vibrations are similar to those for varying R discussed above in Sec. V A 1. The difference in the stiffnesses of specific external forces ($f_1^{(\gamma)} \neq f_2^{(\gamma)}$) at fixed $f_{ji}^{(\gamma)}$ leads to the fact that with increasing

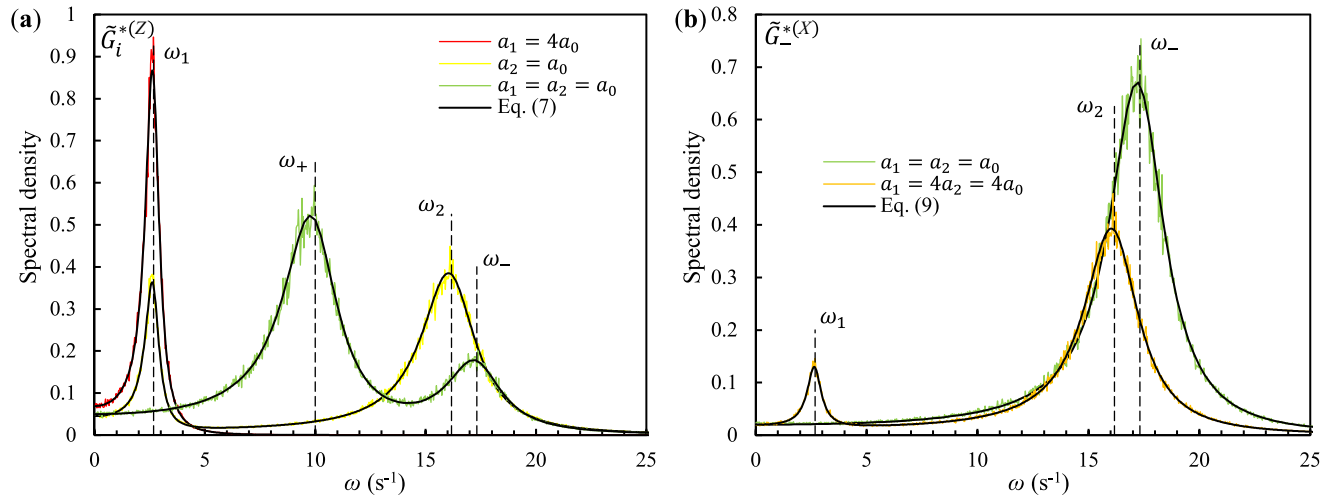

FIG. 6. Normalized spectral densities of (a) $\tilde{G}_i^{*(Z)}$ $(i = 1, 2)$ and (b) $\tilde{G}_-^{*(Z)}$ in the vertical direction Z for particles having different sizes ($a_1 = 4a_2 = 4a_0$) with corresponding changes in other parameters ($m_1 = 64m_2 = 64m_0$, $q_1 = 4q_2 = 4q_0$, $4\nu_1 = \nu_2 = \nu_0$) at $R = 0$, $\alpha/\beta = 4$, $\omega_{t_0}^{(X)} = 20\,\mathrm{s}^{-1}$, $\omega_{t_0}^{(Z)} = 10\,\mathrm{s}^{-1}$, $\nu_0 = 3\,\mathrm{s}^{-1}$. For comparison the case of $\tilde{G}_1^{*(\gamma)} \equiv \tilde{G}_2^{*(\gamma)}$ and $\tilde{G}_-^{*(Z)}$ for $a_1 = a_2 = a_0$ is also shown. The black lines show the analytical solutions (7) and (9), the colored lines show the results of numerical simulation, the dotted lines indicate the main frequencies $\omega_+^{(\gamma)}$ (15), $\omega_-^{(\gamma)}$ (16), $\omega_1^{(\gamma)}$, and $\omega_2^{(\gamma)}$ (12).

$f_i^{(\gamma)}/f_j^{(\gamma)} > 1$, the peak close to zero decreases for the ith particle to visual indefinability, and for the jth particle, the peak far from zero decreases, while the second peak $\omega_-^{(\gamma)}$ and $\omega_+^{(\gamma)}$ appears on the spectra of combined and relative vibrations, respectively. Figure 6 illustrates the effect discussed here with the example of unequal particles for which $f_2^{(Z)}/f_1^{(Z)} = 16$ and $f_{12}^{(Z)}/f_{21}^{(Z)} = 64$. In Fig. 6(a), only the peak closest to zero remains in the spectrum of the lower particle ($i = 1$), while both peaks are present in the spectrum of the upper particle ($i = 2$). The second peak appeared on the spectrum of relative displacements of particles, which is a manifestation of the existing inequality in the derivatives of specific external forces; see Fig. 6(b).

B. Validation of the force measurement technique and its comparison with other methods

We have shown above that the spectral densities of a system of interacting particles are a reflection of the parameters characterizing the system, and their change leads to noticeable transformations of the spectra. Therefore, solving the inverse problem for the spectral densities makes it possible to determine the parameters of the system with high accuracy. Let us consider the reconstruction of the stiffnesses of specific forces in equilibrium positions of particles and friction coefficients with an example of a numerical experiment using the proposed method and other nonperturbative methods and their comparison. Note that in some cases, determining the stiffnesses allows us to make a good estimate of the forces themselves [17]. The analysis was carried out in a wide range of parameters: the friction coefficient varied from 0.1 to 100 s^{-1}, and for each friction a series of calculations was carried out in the range of R varying from 0 to 10. Ultimately, for each set of parameters $\varrho = \nu/\omega_t^{(\gamma)}$ and R, the stiffnesses of specific forces and friction coefficients were restored using various methods, namely, the spectral response to stochastic processes (SRSP) method using the velocity spectral densities described in Sec. III, the scanning mode spectra (SMS) method [57,58], solving the inverse Langevin problem (ILP) [54,56], and correlational analysis of random motion (CARM) [59,60]. For each value of ϱ, the maximum recovery errors were found among all the values of R. The above methods were applied both for pure (un-noised) particle trajectories obtained from the Langevin molecular dynamics simulations and for the same trajectories with additional noise superimposed on them, simulating experimental errors in determining the positions of particles [see Eq. (19)]. The results obtained are presented in Fig. 7 .

In Figs. 7(a) and 7(c) all the considered methods applied to the pure trajectories demonstrate an expected deterioration in the accuracy of force recovery with increasing friction, while the ILP method shows the smallest error: less than 3% and 4.5% for the external and interparticle forces, respectively, almost over the entire range of ϱ considered. Since friction is not taken into account in the SMS method, it has the largest error exceeding 10% at $\varrho > 0.6$ and 0.1 for external and interparticle forces, respectively. The maximum error is ∼10% for the SRSP method versus ∼30% for the CARM method.

Figures 7(b) and 7(d) present errors in determination of the specific force stiffnesses in the two-particle system obtained by applying different methods to the trajectories with additional noise due to the particle position measurement errors. We point out that the accuracy of system parameter recovery using the SMS and SRSP methods has not changed. Thus, methods based on the analysis of vibration spectra are not sensitive to the measurement random errors provided that the data are sufficiently averaged. Note that the random error in formula (19) shows up as a constant addition $\sim p^2\Delta t$ [here p is the standard deviation in (19) and Δt is integration step in simulation] on the spectral density of displacements, and as a quadratic function $\sim\omega^2\, p^2\, \Delta t$ in the velocity spectra, which is only less than 0.1% and 1.5% of the amplitudes of the spectral densities in the considered frequency range, respectively. However, this measurement error is the main limitation for the nonspectral methods (ILP and CARM): over the entire friction range considered, the average recovery error is ∼25% for the external forces, and ∼40% for the interparticle forces.

Determining friction from the pure trajectories shows the following maximum error: ∼3% for the ILP, from 25% to 2.5% with increasing ϱ for the SRSP method, and from 0.5% to 50% for the CARM method. However, in the case of the noisy trajectories due to the particle position measurement errors, the friction error of the SRSP method does not change, but for the CARM method it increases to ∼39%, and ILP does not recover friction at all.

Note that in the work of SRSP, a dependence of the reconstruction error on the value of R is observed: there is a decrease in the error with an increase in the nonreciprocity from $R = 1$. The greater ϱ is, the more pronounced is the dependence: an example in Fig. 8 shows the errors in determining the specific force stiffness in the X and Z directions at $\varrho^{(X)} = \nu/\omega_t^{(X)} = 5$ and $\varrho^{(Z)} = \nu/\omega_t^{(Z)} = 10$ where $\nu = 100\,\mathrm{s}^{-1}$. As can be seen, there is a decrease in the error of the specific interaction force stiffness: from 7.5% to less than 3% for $f_{ji}^{(X)}$, and from about 12% to less than 5% for $f_{ji}^{(Z)}$. This effect is associated with an increase in the absolute values of the derivatives of the specific interparticle forces $|f_{ji}^{(\gamma)}|$ with increasing R, which is also manifested visually in an increase in the amplitude of the peaks; see Fig. 1. The influence of R at large ϱ is described in more detail in Sec. V A 2. An increase in the error of the specific external force stiffness $f_i^{(Z)}$ is associated with a significant decrease in the relative value of specific force derivatives in the Z direction: $(f_1^{(Z)} + f_2^{(Z)})/(|f_{21}^{(Z)}| + |f_{21}^{(Z)}|) = 1$ and 0.1 for $R = 0$ and 10, respectively.

Note that microparticles immersed in a low-pressure gas discharge acquire significantly higher effective kinetic temperatures (up to 10–10^5 times) compared to the ambient gas temperature [85,92–96]. It is assumed that high kinetic heating is a collective phenomenon associated with wake-induced instabilities [36,96–102] and fluctuations of microparticle charges [103–107]. However, the effective temperature of even a single microparticle can be several times higher than the ambient gas temperature quantifying the intensity of classical Brownian motion [82,108,109]. The most commonly discussed mechanism of stochastic heating of a single dust particle in a plasma is the charge fluctuation

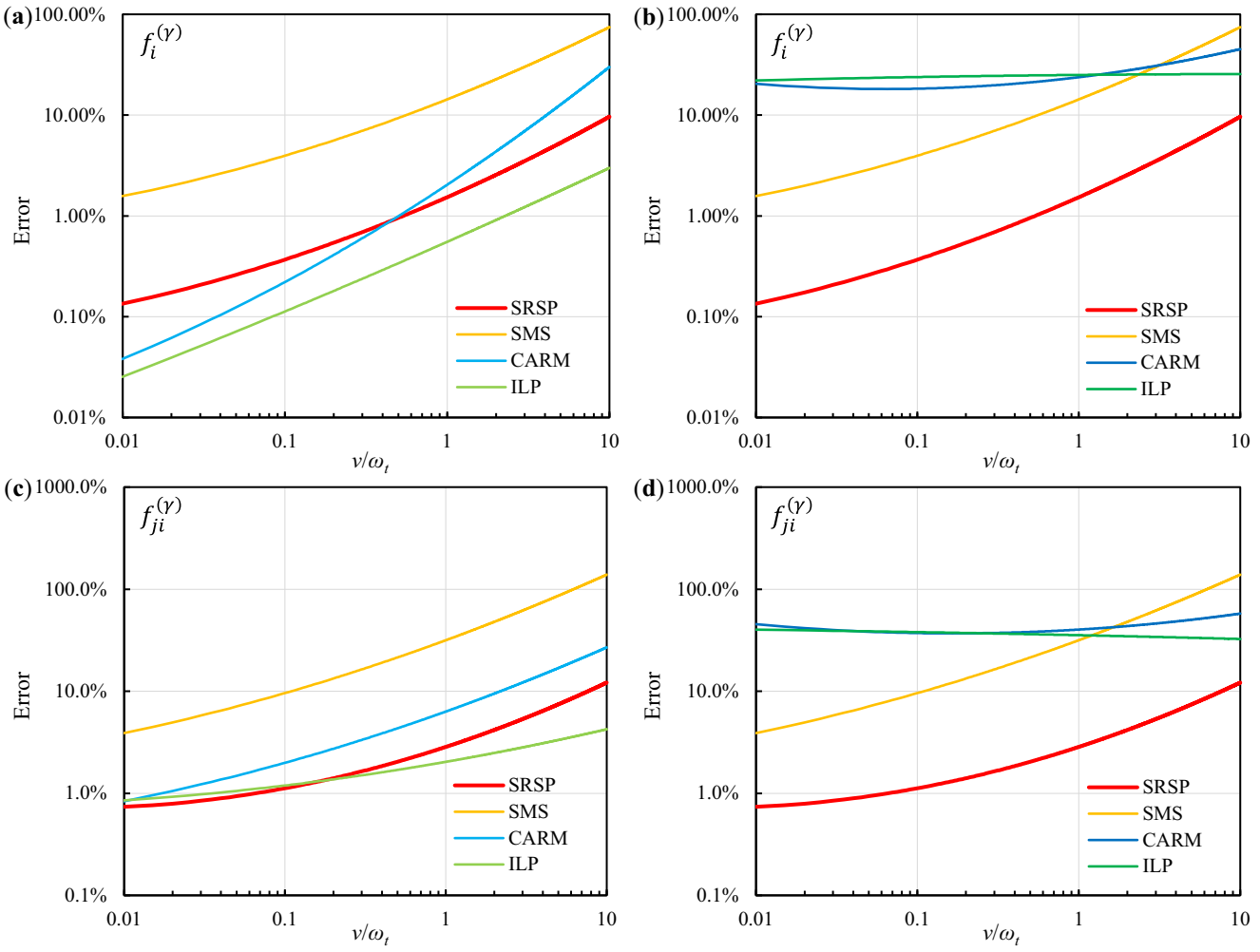

FIG. 7. Maximum errors in determination of the stiffnesses of the specific (a,b) external and (c,d) interparticle forces in the equilibrium positions of particles for a system of two nonreciprocally interacting particles in a trap. For comparison, the four nonperturbative methods, namely, the spectral response to stochastic processes (SRSP), the scanning mode spectra (SMS), the correlational analysis of random motion (CARM), and the inverse Langevin problem (ILP) were applied both (a,c) for the pure particle trajectories obtained from the Langevin molecular dynamics simulations and (b,d) for the same trajectories with additional noise superimposed on them, simulating experimental errors in determining the positions of particles [see Eq. (19)]. For each ratio of ν/ω_t, the maximum error was chosen among the results obtained for the X and Z directions, and for particles with the nonreciprocity ranging from $R = 0$ to 10.

[34,82,87,94,105,107,110,111] caused by the granularity (discreteness) and random nature of the incoming fluxes of ions and electrons charging the particle [112–117]. Thus, the average kinetic energy in a system of particles is the sum of effective thermal energy due to some translational noise and additional energy supply due to collective effects.

Note that, unlike the other methods, SRSP allows us to determine precisely the noise-induced temperatures of the effective Brownian motion of particles (i.e., heat sources), that can be smaller than the total effective kinetic temperature of the particles. This feature is important in studying the wake-induced heating of dust particles [6,69,86]. The SRSP method also avoids the influence of systematic errors that are manifested as "parasitic" modes, in particular, the movement of a system of particles as a whole or any processing artifacts. A preliminary analysis of the spectral density makes it possible to allocate for the SRSP method a frequency section with only a useful signal, if this section is not superimposed by "parasitic" modes.

VI. CONCLUSION

An analytical and numerical study of the spectral characteristics of stochastic motion in an underdamped system of confined particles with effective violation of the interparticle interaction symmetry has been carried out.

A unique method of spectral response to stochastic processes (SRSP) for diagnostics of interaction forces between strongly coupled microparticles in a colloidal plasma was proposed. We note the main advantages of the method:

(i) absence of necessity for external perturbations of the system and no special design of the experimental setup is required;

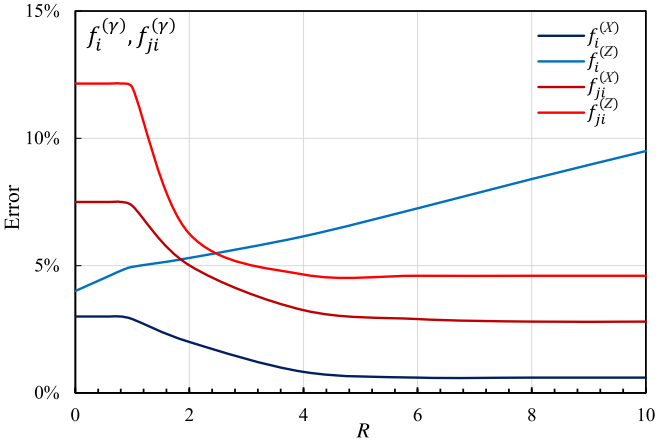

FIG. 8. Errors in determining the stiffnesses of the specific external $f_i^{(\gamma)}$ and interparticle $f_{ji}^{(\gamma)}$ forces in the equilibrium positions of particles in the X and Z directions obtained by applying the SRSP method to the particle trajectories at $\nu = 100\,\mathrm{s}^{-1}$ ($\nu/\,\omega_t^{(X)} = 5$ and $\nu/\,\omega_t^{(Z)} = 10$).

(ii) absence of necessity for preliminary measurements and assumptions about external fields, about the type of interaction, and the particle sizes;

(iii) applicability to systems consisting of different sorts of particles with different sizes, charges, and kinetic temperatures, and with any type of interparticle interaction;

(iv) ability, along with the measurement of stiffnesses of specific interparticle forces in equilibrium positions of particles, to determine the stiffnesses of specific external forces in equilibrium positions and friction coefficients for each particle, which makes it possible to determine particle sizes using the Epstein formula [118];

(v) possibility to determine the noise-induced temperatures of the particles (thermal sources) corresponding to their stochastic motion without taking into account the influence of neighboring particles;

(vi) applicability to moderately overdamped systems in case of sufficient nonreciprocity.

The comparison with other nonperturbative methods showed significant advantages of the method, especially when processing particle trajectories with errors in measuring their positions in space.

In conclusion, we note that the SRSP method makes it possible to quantitatively analyze interaction forces, allowing us to study nonreciprocal systems of various natures. Also, combined with the ability of measuring the noise-induced kinetic temperatures of particles, the method permits experimental testing of various theoretical and numerical heating models, helping us pinpoint the exact mechanisms behind the anomalous kinetic heating of particles.

ACKNOWLEDGMENT

This work was supported by the Russian Science Foundation under Grant No. 19-12-00354.

APPENDIX A: BASIC EQUATIONS FOR A SYSTEM OF COUPLED OSCILLATORS

Consider a generalized linear system of N asymmetrically (nonreciprocally) coupled oscillators $\delta_i(t)$ driven by some processes $B_i(t)$:

$$\frac{d^2\delta_i}{dt^2} = -\sum_{j=1}^{N} u_{ij}\frac{d\delta_j}{dt} + \sum_{j=1}^{N} a_{ij}\delta_j + B_i, \tag{A1}$$

where u_{ij} are the generalized friction coefficients, and the coefficients a_{ij} depend on the physics of the problem being solved. The processes $B_i(t)$ operating in the system (A1) are characterized by the spectral density,

$$S_i(\omega) = 2\int_0^\infty \langle B_i(t)B_i(t+\tau)\rangle \cos\omega\tau d\tau, \tag{A2}$$

and the cross-spectral density,

$$S_{ij}(\omega) = 2\int_0^\infty \langle B_i(t)B_j(t+\tau)\rangle \cos\omega\tau d\tau. \tag{A3}$$

Angle brackets $\langle\cdots\rangle$ denote time averaging.

If the system (A1) is under the action of external periodic forces $B_i = H_i \sin\omega t$, then forced oscillations of the form $\delta_i(t) = M_i e^{i\omega t}$ will occur in it, where the coefficients M_i are determined from the system of linear equations $\mathbf{AM} = \mathbf{H}$:

$$\begin{pmatrix} -\omega^2 + i\omega u_{11} - a_{11} & i\omega u_{12} - a_{12} & \vdots & i\omega u_{1N} - a_{1N} \\ i\omega u_{21} - a_{21} & -\omega^2 + i\omega u_{22} - a_{22} & \vdots & i\omega u_{2N} - a_{2N} \\ \cdots & \cdots & \ddots & \cdots \\ i\omega u_{N1} - a_{N1} & i\omega u_{N2} - a_{N2} & \vdots & -\omega^2 + i\omega u_{NN} - a_{NN} \end{pmatrix} \begin{pmatrix} M_1 \\ M_2 \\ \cdots \\ M_N \end{pmatrix} = \begin{pmatrix} H_1 \\ H_2 \\ \cdots \\ H_N \end{pmatrix}. \tag{A4}$$

To solve this system, you can use the Cramer method [119]:

$$M_i = \frac{1}{\det \mathbf{A}} \det \begin{pmatrix} -\omega^2 + i\omega u_{11} - a_{11} & \vdots & i\omega u_{1(i-1)} - a_{1(i-1)} & H_1 & \vdots & i\omega u_{1N} - a_{1N} \\ i\omega u_{21} - a_{21} & \vdots & i\omega u_{2(i-1)} - a_{2(i-1)} & H_2 & \vdots & i\omega u_{2N} - a_{2N} \\ \cdots & \ddots & \cdots & \cdots & \ddots & \cdots \\ i\omega u_{N1} - a_{N1} & \vdots & i\omega u_{N(i-1)} - a_{N(i-1)} & H_N & \vdots & -\omega^2 + i\omega u_{NN} - a_{NN} \end{pmatrix}. \tag{A5}$$

Assuming $H_k = 1$, and the remaining $H_i = 0$ in the expression for M_l, we can determine the frequency transfer function that relates the impact on the kth particle with the response of the lth particle.

Recall that if a stationary random process with a zero mean value is fed to the input of a linear system, then the spectral density $G(\omega)$ of the stationary random process at the output of the linear system is equal to the product of the spectral density $S(\omega)$ of the random process at the input of the system and the square of the modulus of the frequency transfer function $|M|^2$ of this system [73]. If the process B_i acting in the system (A1) on the ith oscillator is stationary, random with $\langle B_i(t)\rangle = 0$, then the spectral density of forced oscillations of the ith oscillator can be represented as

$$G_i(\omega) = \sum_{j=1}^{N} S_j \bar{M}_i(j) + \sum_{j=1}^{N-1}\sum_{k=j+1}^{N} S_{ij}\bar{M}_i(j,k), \tag{A6}$$

where $\bar{M}_i(j) = |M_i(\omega, H_{l,l\neq j}=0, H_j=1)|^2$, and $\bar{M}_i(j,k) = M_i(\omega, H_{l,l\neq j}=0, H_j=1)M_i^*(\omega, H_{l,l\neq k}=0, H_k=1) + M_i^*(\omega, H_{l,l\neq j}=0, H_j=1)M_i(\omega, H_{l,l\neq k}=0, H_k=1)$ ("*" denotes a complex conjugate value).

APPENDIX B: SYSTEM OF TWO OSCILLATORS

We obtain a particular solution for the system (A1) for two oscillators:

$$G_1(\omega) = \frac{S_1\left[(\omega^2+a_{22})^2 + u_{22}^2\omega^2\right] + S_2\left(a_{12}^2 + u_{12}^2\omega^2\right) - 2S_{12}[(a_{12}+u_{22}u_{12})\omega^2 + a_{12}a_{22}]}{W}, \tag{B1}$$

$$G_2(\omega) = \frac{S_1\left[a_{21}^2 + u_{21}^2\omega^2\right] + S_2\left[(\omega^2+a_{11})^2 + u_{11}^2\omega^2\right] - 2S_{12}[(a_{21}+u_{11}u_{21})\omega^2 + a_{11}a_{21}]}{W}, \tag{B2}$$

where

$$W = [\omega^4 + \omega^2(u_{12}u_{21} - u_{11}u_{22} + a_{11} + a_{22}) + a_{11}a_{22} - a_{12}a_{21}]^2 + \omega^2[\omega^2(u_{11}+u_{22}) + u_{22}a_{11} + u_{11}a_{22} - u_{12}a_{21} - u_{21}a_{12}]^2. \tag{B3}$$

If the relations for friction $u_{11} = u_{22} = \nu$, $u_{12} = u_{21} = 0$ are known, then expressions (B1)–(B3) are simplified:

$$G_{1(2)}(\omega) = \frac{S_{1(2)}[(\omega^2 + a_{22(11)})^2 + \nu^2\omega^2] + S_{2(1)}a_{12(21)}^2 - 2S_{12}[a_{12(21)}\omega^2 + a_{12(21)}a_{22(11)}]}{\left[\omega^4 + \left(\nu^2 - 2\omega_1^2\right)\omega^2 + \omega_1^4\right]\left[\omega^4 + \left(\nu^2 - 2\omega_2^2\right)\omega^2 + \omega_2^4\right]}, \tag{B4}$$

where

$$\omega_{1(2)}^2 = -\frac{a_{11}+a_{22}}{2} \mp \frac{\sqrt{(a_{11}-a_{22})^2 + 4a_{12}a_{21}}}{2}. \tag{B5}$$

APPENDIX C: SYSTEM OF INTERACTING BROWNIAN PARTICLES

The description of the system of interacting Brownian particles and the corresponding spectral densities (5) is presented in Sec. II A. To obtain expressions (5), it is necessary to carry out calculations similar to Appendix A with respect to the new system of equations obtained by transforming system (A1), for displacements $\xi_i^{(\gamma)}$ with coefficients $b_{ij}^{(\gamma)}$ ($\delta_i \to \xi_i^{(\gamma)}$, $a_{ij} \equiv b_{ij}^{(\gamma)}$, $u_{ii} \equiv \nu_i$, $u_{ij,\ i\neq j} \equiv 0$). The coefficients $b_{ij}^{(\gamma)}$ are related to the values of the derivatives of the specific external and interparticle forces using

$$b_{ii}^{(\gamma)} = \sum_{j=1,\, j\neq i}^{N} f_{ji}^{(\gamma)} - f_i^{(\gamma)}, \quad b_{ij,\ i\neq j}^{(\gamma)} = -f_{ji}^{(\gamma)}. \tag{C1}$$

Also, using a similar approach for the system of equations (A1), one can obtain the spectral densities of combined and relative displacements of particles:

$$\begin{aligned}
\eta_1^{(\gamma)} &= \xi_1^{(\gamma)} - \xi_2^{(\gamma)} \\
&\cdots \\
\eta_i^{(\gamma)} &= \xi_i^{(\gamma)} - \xi_{i+1}^{(\gamma)} \\
&\cdots \\
\eta_{N-1}^{(\gamma)} &= \xi_{N-1}^{(\gamma)} - \xi_N^{(\gamma)} \\
\eta_N^{(\gamma)} &= \sum_{j=1}^{N} \xi_j^{(\gamma)}.
\end{aligned} \tag{C2}$$

Thus, we obtain a new system of equations for $\eta_i^{(\gamma)}$ with coefficients $\mathrm{c}_{ij}^{(\gamma)}$ ($\delta_i \to \eta_i^{(\gamma)}$, $a_{ij} \equiv \mathrm{c}_{ij}^{(\gamma)}$, u_{ij}) under the influence of new Langevin forces $F_{\mathrm{ran},i}^{'(\gamma)}$, while the coefficients u_{ij}, $\mathrm{c}_{ij}^{(\gamma)}$ are related to the original ν_i, $b_{ij}^{(\gamma)}$ by systems of linear equations:

$$\begin{pmatrix} -u_{11}-u_{1N} & u_{11}-u_{12}-u_{1N} & \vdots & u_{1(i-1)}-u_{1i}-u_{1N} & \vdots & u_{1(N-1)}-u_{1N} \\ -u_{21}-u_{2N} & u_{21}-u_{22}-u_{2N} & \vdots & u_{2(i-1)}-u_{2i}-u_{2N} & \vdots & u_{2(N-1)}-u_{2N} \\ \cdots & \cdots & \ddots & \cdots & \ddots & \cdots \\ -u_{N1}-u_{NN} & u_{N1}-u_{N2}-u_{NN} & \vdots & u_{N(i-1)}-u_{Ni}-u_{NN} & \vdots & u_{N(N-1)}-u_{NN} \end{pmatrix}$$
$$= \begin{pmatrix} -\nu_1 & \nu_2 & 0 & \vdots & 0 & 0 \\ 0 & -\nu_2 & \nu_3 & \vdots & 0 & 0 \\ \cdots & \cdots & \cdots & \ddots & \cdots & \cdots \\ 0 & 0 & 0 & \vdots & -\nu_{N-1} & \nu_N \\ -\nu_1 & -\nu_2 & -\nu_3 & \vdots & -\nu_{N-1} & -\nu_N \end{pmatrix}, \tag{C3}$$

$$\begin{pmatrix} c_{11}^{(\gamma)}+c_{1N}^{(\gamma)} & c_{12}^{(\gamma)}-c_{11}^{(\gamma)}+c_{1N}^{(\gamma)} & \vdots & c_{1i}^{(\gamma)}-c_{1(i-1)}^{(\gamma)}+c_{1N}^{(\gamma)} & \vdots & c_{1N}^{(\gamma)}-c_{1(N-1)}^{(\gamma)} \\ c_{21}^{(\gamma)}+c_{2N}^{(\gamma)} & c_{22}^{(\gamma)}-c_{21}^{(\gamma)}+c_{2N}^{(\gamma)} & \vdots & c_{2i}^{(\gamma)}-c_{2(i-1)}^{(\gamma)}+c_{2N}^{(\gamma)} & \vdots & c_{2N}^{(\gamma)}-c_{2(N-1)}^{(\gamma)} \\ \cdots & \cdots & \ddots & \cdots & \ddots & \cdots \\ c_{N1}^{(\gamma)}+c_{NN}^{(\gamma)} & c_{N2}^{(\gamma)}-c_{N1}^{(\gamma)}+c_{NN}^{(\gamma)} & \vdots & c_{Ni}^{(\gamma)}-c_{N(i-1)}^{(\gamma)}+c_{NN}^{(\gamma)} & \vdots & c_{NN}^{(\gamma)}-c_{N(N-1)}^{(\gamma)} \end{pmatrix}$$
$$= \begin{pmatrix} b_{11}^{(\gamma)}-b_{21}^{(\gamma)} & b_{12}^{(\gamma)}-b_{22}^{(\gamma)} & \vdots & b_{1i}^{(\gamma)}-b_{2i}^{(\gamma)} & \vdots & b_{1N}^{(\gamma)}-b_{2N}^{(\gamma)} \\ b_{21}^{(\gamma)}-b_{31}^{(\gamma)} & b_{22}^{(\gamma)}-b_{32}^{(\gamma)} & \vdots & b_{2i}^{(\gamma)}-b_{3i}^{(\gamma)} & \vdots & b_{2N}^{(\gamma)}-b_{3N}^{(\gamma)} \\ \cdots & \cdots & \ddots & \cdots & \ddots & \cdots \\ b_{(N-1)1}^{(\gamma)}-b_{N1}^{(\gamma)} & b_{(N-1)2}^{(\gamma)}-b_{N2}^{(\gamma)} & \vdots & b_{(N-1)i}^{(\gamma)}-b_{Ni}^{(\gamma)} & \vdots & b_{(N-1)N}^{(\gamma)}-b_{NN}^{(\gamma)} \\ \sum_{j=1}^{N} b_{j1}^{(\gamma)} & \sum_{j=1}^{N} b_{j2}^{(\gamma)} & \vdots & \sum_{j=1}^{N} b_{ji}^{(\gamma)} & \vdots & \sum_{j=1}^{N} b_{jN}^{(\gamma)} \end{pmatrix} \tag{C4}$$

For the system under consideration, the spectral densities $S_{\eta_i}^{(\gamma)}$ have the following values: $S_{\eta_i, i\neq N}^{(\gamma)} = S_{\xi_i}^{(\gamma)} + S_{\xi_{i+1}}^{(\gamma)}$, while $S_{\eta_N}^{(\gamma)} = \sum_{j=1}^{N} S_{\xi_j}^{(\gamma)}$. If previously $F_{\mathrm{ran},i}^{(\gamma)}$ were independent, then $F_{\mathrm{ran},i}^{'(\gamma)}$ have a cross-spectral density, $S_{\eta_i\eta_j, i\neq j\neq N}^{(\gamma)} = -S_{\xi_k}^{(\gamma)}$, where $k = \max(i, j)$ if $|i-j| = 1$; otherwise $S_{\eta_i\eta_j, i\neq j\neq N}^{(\gamma)} = 0$, and $S_{\eta_i\eta_N, i\neq N}^{(\gamma)} = S_{\xi_i}^{(\gamma)} - S_{\xi_{i+1}}^{(\gamma)}$.

Transforming (A6), we obtain the spectral density distribution for $\eta_i^{(\gamma)}$:

$$G_{\eta_i}^{(\gamma)}(\omega) = \sum_{j=1}^{N} S_{\eta_j}^{(\gamma)} \bar{M}_{\eta_i}^{(\gamma)}(j) + \sum_{j=1}^{N-1} S_{\eta_j\eta_N}^{(\gamma)} \bar{M}_{\eta_i}^{(\gamma)}(j, N) + \sum_{j=1}^{N-2} S_{\eta_j\eta_{j+1}}^{(\gamma)} \bar{M}_{\eta_i}^{(\gamma)}(j, j+1). \tag{C5}$$

[1] V. A. Schweigert, I. V. Schweigert, A. Melzer, A. Homann, and A. Piel, Plasma crystal melting: A nonequilibrium phase transition, Phys. Rev. Lett. **80**, 5345 (1998).

[2] K. Hayashi and S. Sasa, The law of action and reaction for the effective force in a non-equilibrium colloidal system, J. Phys.: Condens. Matter **18**, 2825 (2006).

[3] H. J. Kronzucker, M. W. Szczerba, L. M. Schulze, and D. T. Britto, Non-reciprocal interactions between K^+ and Na^+ ions in barley (*Hordeum vulgare* L.), J. Exp. Bot. **59**, 2793 (2008).

[4] R. Fleury, D. L. Sounas, C. F. Sieck, M. R. Haberman, and A. Alù, Sound isolation and giant linear nonreciprocity in a compact acoustic circulator, Science **343**, 516 (2014).

[5] S. Sukhov, A. Shalin, D. Haefner, and A. Dogariu, *Actio et reactio* in optical binding, Opt. Express **23**, 247 (2015).

[6] A. V. Ivlev, J. Bartnick, M. Heinen, C.-R. Du, V. Nosenko, and H. Löwen, Statistical mechanics where Newton's third law is broken, Phys. Rev. X **5**, 011035 (2015).

[7] O. S. Vaulina, I. I. Lisina, and E. A. Lisin, Energy exchange in systems of particles with nonreciprocal interaction, J. Exp. Theor. Phys. **121**, 717 (2015).

[8] A. Metelmann and A. A. Clerk, Nonreciprocal photon transmission and amplification via reservoir engineering, Phys. Rev. X **5**, 021025 (2015).

[9] J. Bartnick, M. Heinen, A. V. Ivlev, and H. Löwen, Structural correlations in diffusiophoretic colloidal mixtures with nonreciprocal interactions, J. Phys.: Condens. Matter **28**, 025102 (2016).

[10] C. Coulais, D. Sounas, and A. Alù, Static non-reciprocity in mechanical metamaterials, Nature (London) **542**, 461 (2017).
[11] N. P. Kryuchkov, A. V. Ivlev, and S. O. Yurchenko, Dissipative phase transitions in systems with nonreciprocal effective interactions, Soft Matter **14**, 9720 (2018).
[12] C. Caloz, A. Alù, S. Tretyakov, D. Sounas, and K. Achouri, and Z.-L. Deck-Léger, Electromagnetic nonreciprocity, Phys. Rev. Appl. **10**, 047001 (2018).
[13] F. A. Lavergne, H. Wendehenne, T. Bäuerle, and C. Bechinger, Group formation and cohesion of active particles with visual perception–dependent motility, Science **364**, 70 (2019).
[14] S. Saha, S. Ramaswamy, and R. Golestanian, Pairing, waltzing and scattering of chemotactic active colloids, New J. Phys. **21**, 063006 (2019).
[15] M. Brandenbourger, X. Locsin, E. Lerner, and C. Coulais, Non-reciprocal robotic metamaterials, Nat. Commun. **10**, 4608 (2019).
[16] J. Agudo-Canalejo and R. Golestanian, Active phase separation in mixtures of chemically interacting particles, Phys. Rev. Lett. **123**, 018101 (2019).
[17] E. A. Lisin, O. F. Petrov, E. A. Sametov, O. S. Vaulina, K. B. Statsenko, M. M. Vasiliev, J. Carmona-Reyes, and T. W. Hyde, Experimental study of the nonreciprocal effective interactions between microparticles in an anisotropic plasma, Sci. Rep. **10**, 13653 (2020).
[18] S. A. M. Loos and S. H. L. Klapp, Irreversibility, heat and information flows induced by non-reciprocal interactions, New J. Phys. **22**, 123051 (2020).
[19] H. Nassar, B. Yousefzadeh, R. Fleury, M. Ruzzene, A. Alù, C. Daraio, A. N. Norris, G. Huang, and M. R. Haberman, Nonreciprocity in acoustic and elastic materials, Nat. Rev. Materials **5**, 667 (2020).
[20] Z. You, A. Baskaran, and M. C. Marchetti, Nonreciprocity as a generic route to traveling states, Proc. Natl. Acad. Sci. USA **117**, 19767 (2020).
[21] S. Saha, J. Agudo-Canalejo, and R. Golestanian, Scalar active mixtures: The nonreciprocal Cahn-Hilliard model, Phys. Rev. X **10**, 041009 (2020).
[22] F. Jiménez-Ángeles, K. J. Harmon, T. D. Nguyen, P. Fenter, and M. Olvera de la Cruz, Nonreciprocal interactions induced by water in confinement, Phys. Rev. Res. **2**, 043244 (2020).
[23] N. P. Kryuchkov, L. A. Mistryukova, A. V. Sapelkin, and S. O. Yurchenko, Strange attractors induced by melting in systems with nonreciprocal effective interactions, Phys. Rev. E **101**, 063205 (2020).
[24] V. S. Nikolaev and A. V. Timofeev, Nonhomogeneity of phase state in a dusty plasma monolayer with nonreciprocal particle interactions, Phys. Plasmas **28**, 033704 (2021).
[25] M. Fruchart, R. Hanai, P. B. Littlewood, and V. Vitelli, Nonreciprocal phase transitions, Nature (London) **592**, 363 (2021).
[26] B. Sabass and U. Seifert, Efficiency of surface-driven motion: Nanoswimmers beat microswimmers, Phys. Rev. Lett. **105**, 218103 (2010).
[27] R. Soto and R. Golestanian, Self-assembly of catalytically active colloidal molecules: Tailoring activity through surface chemistry, Phys. Rev. Lett. **112**, 068301 (2014).
[28] S. A. Mallory, F. Alarcon, A. Cacciuto, and C. Valeriani, Self-assembly of active amphiphilic Janus particles, New J. Phys. **19**, 125014 (2017).
[29] J. Dzubiella, H. Löwen, and C. N. Likos, Depletion forces in nonequilibrium, Phys. Rev. Lett. **91**, 248301 (2003).
[30] A. S. Khair and J. F. Brady, On the motion of two particles translating with equal velocities through a colloidal dispersion, Proc. R. Soc. A **463**, 223 (2007).
[31] C. Mejía-Monasterio and G. Oshanin, Bias- and bath-mediated pairing of particles driven through a quiescent medium, Soft Matter **7**, 993 (2011).
[32] I. Sriram and E. M. Furst, Out-of-equilibrium forces between colloids, Soft Matter **8**, 3335 (2012).
[33] S. Steffenoni, K. Kroy, and G. Falasco, Interacting Brownian dynamics in a nonequilibrium particle bath, Phys. Rev. E **94**, 062139 (2016).
[34] G. E. Morfill and A. V. Ivlev, Complex plasmas: An interdisciplinary research field, Rev. Mod. Phys. **81**, 1353 (2009).
[35] A. V. Ivlev and R. Kompaneets, Instabilities in bilayer complex plasmas: Wake-induced mode coupling, Phys. Rev. E **95**, 053202 (2017).
[36] I. I. Lisina and O. S. Vaulina, Formation of layered structures of particles with anisotropic pair interaction, EPL **103**, 55002 (2013).
[37] J. Bartnick, A. Kaiser, H. Löwen, and A. V. Ivlev, Emerging activity in bilayered dispersions with wake-mediated interactions, J. Chem. Phys. **144**, 224901 (2016).
[38] A. V. Filippov and I. N. Derbenev, Effect of the size of charged spherical macroparticles on their electrostatic interaction in an equilibrium plasma, J. Exp. Theor. Phys. **123**, 1099 (2016).
[39] A. M. Ignatov, Lesage gravity in dusty plasmas, Plasma Phys. Rep. **22**, 585 (1996).
[40] Ya. K. Khodataev, G. E. Morfill, and V. N. Tsytovich, Role of neutral-particle bombardment in dust–dust interactions in plasmas, J. Plasma Phys. **65**, 257 (2001).
[41] S. A. Khrapak, A. V. Ivlev, and G. Morfill, Interaction potential of microparticles in a plasma: Role of collisions with plasma particles, Phys. Rev. E **64**, 046403 (2001).
[42] A. D. Usachev, A. V. Zobnin, O. F. Petrov, V. E. Fortov, B. M. Annaratone, M. H. Thoma, H. Höfner, M. Kretschmer, M. Fink, and G. E. Morfill, Formation of a boundary-free dust cluster in a low-pressure gas-discharge plasma, Phys. Rev. Lett. **102**, 045001 (2009).
[43] A. Melzer, V. A. Schweigert, and A. Piel, Transition from attractive to repulsive forces between dust molecules in a plasma sheath, Phys. Rev. Lett. **83**, 3194 (1999).
[44] I. H. Hutchinson, Intergrain forces in low-Mach-number plasma wakes, Phys. Rev. E **85**, 066409 (2012).
[45] R. Kompaneets, G. E. Morfill, and A. V. Ivlev, Wakes in complex plasmas: A self-consistent kinetic theory, Phys. Rev. E **93**, 063201 (2016).
[46] G. I. Sukhinin, A. V. Fedoseev, M. V. Salnikov, A. Rostom, M. M. Vasiliev, and O. F. Petrov, Plasma anisotropy around a dust particle placed in an external electric field, Phys. Rev. E **95**, 063207 (2017).
[47] H. Jung, F. Greiner, O. H. Asnaz, J. Carstensen, and A. Piel, Exploring the wake of a dust particle by a continuously approaching test grain, Phys. Plasmas **22**, 053702 (2015).
[48] K. Takahashi, T. Oishi, K. Shimomai, Y. Hayashi, and S. Nishino, Analyses of attractive forces between particles in Coulomb crystal of dusty plasmas by optical manipulations, Phys. Rev. E **58**, 7805 (1998).

[49] M. Chen, M. Dropmann, B. Zhang, L. S. Matthews, and T. W. Hyde, Ion-wake field inside a glass box, Phys. Rev. E **94**, 033201 (2016).

[50] N. J. Prior, L. W. Mitchell, and A. A. Samarian, Determination of charge on vertically aligned particles in a complex plasma using laser excitations, J. Phys. D: Appl. Phys. **36**, 1249 (2003).

[51] M. Kroll, J. Schablinski, D. Block, and A. Piel, On the influence of wakefields on three-dimensional particle arrangements, Phys. Plasmas **17**, 013702 (2010).

[52] G. A. Hebner, M. E. Riley, and B. M. Marder, Dynamic probe of dust wakefield interactions using constrained collisions, Phys. Rev. E **68**, 016403 (2003).

[53] K. S. Ashrafi, R. Yousefi, M. Chen, L. S. Matthews, and T. W. Hyde, Dust as probes: Determining confinement and interaction forces, Phys. Rev. E **102**, 043210 (2020).

[54] O. S. Vaulina, E. A. Lisin, A. V. Gavrikov, O. F. Petrov, and V. E. Fortov, Determination of pair interaction forces between particles in nonideal dissipative systems, Phys. Rev. Lett. **103**, 035003 (2009).

[55] E. A. Lisin and O. S. Vaulina, Influence of external perturbations on dynamical characteristics of dust clusters (simulation), J. Exp. Theor. Phys. **115**, 947 (2012).

[56] E. A. Lisin, I. I. Lisina, O. S. Vaulina, and O. F. Petrov, Solution of the inverse Langevin problem for open dissipative systems with anisotropic interparticle interaction, Phys. Plasmas **22**, 033704 (2015).

[57] K. Qiao, Z. Ding, J. Kong, M. Chen, L. S. Matthews, and T. W. Hyde, Determination of interaction between a dust particle pair in complex plasmas, arXiv:1705.01982.

[58] K. Qiao, Z. Ding, J. Kong, M. Chen, L. S. Matthews, and T. W. Hyde, Non-perturbative experiments on plasma-mediated particle interaction and the ion wake potential, arXiv:1810.07173.

[59] E. A. Lisin, O. S. Vaulina, and O. F. Petrov, Correlational approach to study interactions between dust Brownian particles in a plasma, Phys. Plasmas **25**, 013702 (2018).

[60] E. A. Lisin, O. S. Vaulina, and O. F. Petrov, Verifying the reciprocity of interparticle interaction forces in strongly coupled systems, J. Exp. Theor. Phys. **124**, 678 (2017).

[61] O. S. Vaulina, E. A. Lisin, A. V. Gavrikov, O. F. Petrov, and V. E. Fortov, Analysis of pair interparticle interaction in nonideal dissipative systems, J. Exp. Theor. Phys. **110**, 662 (2010).

[62] E. A. Lisin, R. A. Timirkhanov, O. S. Vaulina, O. F. Petrov, and V. E. Fortov, Influence of external perturbations on the interaction between grains in plasma, New J. Phys. **15**, 053004 (2013).

[63] E. A. Lisin, O. S. Vaulina, O. F. Petrov, and V. E. Fortov, Dust-particle charge in weakly ionized gas-discharge plasma, EPL **97**, 55003 (2012).

[64] E. A. Lisin, O. S. Vaulina, O. F. Petrov, and V. E. Fortov, Contactless methods for studying interactions between dust particles in a gas-discharge plasma, Plasma Phys. Controlled Fusion **55**, 124022 (2013).

[65] A. K. Mukhopadhyay and J. Goree, Experimental measurement of velocity correlations for two microparticles in a plasma with ion flow, Phys. Rev. E **90**, 013102 (2014).

[66] E. A. Lisin, E. A. Kononov, E. A. Sametov, M. M. Vasiliev, and O. F. Petrov, Alignments of a microparticle pair in a glow discharge, Molecules **26**, 7535 (2021).

[67] E. A. Sametov, E. A. Lisin, and O. S. Vaulina, Oscillations of a dissipative system of two non-mutually coupled oscillators under the influence of random forces, Vestn. Obed. Inst. Vys. Temp. **2**, 33 (2019).

[68] E. A. Sametov, E. A. Lisin, and O. S. Vaulina, Spectral characteristics of stochastic motion in the system of two interacting particles, J. Exp. Theor. Phys. **130**, 463 (2020).

[69] O. S. Vaulina, E. A. Sametov, and E. A. Lisin, Spectral characteristics of charged particles in limited chain structures, J. Exp. Theor. Phys. **131**, 361 (2020).

[70] O. S. Vaulina, Spectral characteristics of small cluster systems (chain structures), Plasma Phys. Rep. **46**, 419 (2020).

[71] O. S. Vaulina, E. A. Sametov, E. A. Lisin, and I. I. Lisina, Spectral characteristics of small-sized quasi-two-dimensional clusters, Plasma Phys. Rep. **46**, 1210 (2020).

[72] Yu. L. Klimontovich, *Statistical Physics* (Harwood Academic, New York, 1986).

[73] A. A. Voronov, *Theory of Automatic Control, Part 2* (Vysshaya Shkola, Moscow, 1986).

[74] J. C. Lagarias, J. A. Reeds, M. H. Wright, and P. E. Wright, Convergence properties of the Nelder–Mead simplex method in low dimensions, SIAM J. Optim. **9**, 112 (1998).

[75] A. J. Jerri, The Shannon sampling theorem—its various extensions and applications: A tutorial review, Proc. IEEE **65**, 1565 (1977).

[76] J. Max, *Méthodes et Techniques de Traitement du Signal et Applications aux Mesures Physiques. Tome 2: Appareillages, Méthodes Nouvelles Exemples d'Applications* (Masson, Paris, 1987).

[77] F. J. Harris, On the use of Windows for harmonic analysis with the discrete Fourier transform, Proc. IEEE **66**, 51 (1978).

[78] O. S. Vaulina, O. F. Petrov, V. E. Fortov, A. G. Khrapak, and S. A. Khrapak, *Dusty Plasma: Experiment and Theory* (Fizmatlit, Moscow, 2009).

[79] V. E. Fortov and G. E. Morfill, *Complex and Dusty Plasmas: From Laboratory to Space* (CRC Press/Taylor & Francis, Boca Raton, FL, 2010).

[80] A. Ivlev, H. Löwen, G. Morfill, and C. P. Royall, *Complex Plasmas and Colloidal Dispersions: Particle-Resolved Studies of Classical Liquids and Solids, Vol. 5* (World Scientific, Singapore, 2012).

[81] *Introduction to Complex Plasmas*, edited by M. Bonitz, N. J. M. Horing, and P. Ludwig (Springer, Heidelberg, 2010).

[82] C. Schmidt and A. Piel, Stochastic heating of a single Brownian particle by charge fluctuations in a radio-frequency produced plasma sheath, Phys. Rev. E **92**, 043106 (2015).

[83] U. Konopka, G. E. Morfill, and L. Ratke, Measurement of the interaction potential of microspheres in the sheath of a rf discharge, Phys. Rev. Lett. **84**, 891 (2000).

[84] O. S. Vaulina, I. I. Lisina, and E. A. Lisin, Influence of different kinetic heating mechanisms on the dynamics of a trapped Brownian particle in a complex plasma, Phys. Plasmas **29**, 113703 (2022).

[85] A. Melzer, A. Homann, and A. Piel, Experimental investigation of the melting transition of the plasma crystal, Phys. Rev. E **53**, 2757 (1996).

[86] O. S. Vaulina, I. I. Lisina, and E. A. Lisin, Kinetic energy in a system of particles with a nonreciprocal interaction, EPL **111**, 50003 (2015).

[87] O. S. Vaulina, Influence of inhomogeneous conditions on the kinetic energy of dust macroparticles in plasma, J. Exp. Theor. Phys. **122**, 193 (2016).
[88] N. P. Kryuchkov and S. O. Yurchenko, Collective excitations in active fluids: Microflows and breakdown in spectral equipartition of kinetic energy, J. Chem. Phys. **155**, 024902 (2021).
[89] O. S. Vaulina and E. A. Sametov, Spectral and structural characteristics for cluster systems of charged Brownian particles, J. Exp. Theor. Phys. **127**, 350 (2018).
[90] O. S. Vaulina, Energy exchange in the systems with non-uniform thermal sources, Phys. Plasmas **24**, 023705 (2017).
[91] O. S. Vaulina, Processes of energy exchange in systems of nonidentical particles with inhomogeneous sources of heat, J. Exp. Theor. Phys. **124**, 839 (2017).
[92] H. M. Thomas and G. E. Morfill, Melting dynamics of a plasma crystal, Nature (London) **379**, 806 (1996).
[93] R. Quinn and J. Goree, Single-particle Langevin model of particle temperature in dusty plasmas, Phys. Rev. E **61**, 3033 (2000).
[94] A. Melzer, Mode spectra of thermally excited two-dimensional dust Coulomb clusters, Phys. Rev. E **67**, 016411 (2003).
[95] J. D. Williams and E. Thomas, Initial measurement of the kinetic dust temperature of a weakly coupled dusty plasma, Phys. Plasmas **13**, 063509 (2006).
[96] V. A. Schweigert, I. V. Schweigert, A. Melzer, A. Homann, and A. Piel, Alignment and instability of dust crystals in plasmas, Phys. Rev. E **54**, 4155 (1996).
[97] A. V. Ivlev and G. Morfill, Anisotropic dust lattice modes, Phys. Rev. E **63**, 016409 (2000).
[98] S. K. Zhdanov, A. V. Ivlev, and G. E. Morfill, Mode-coupling instability of two-dimensional plasma crystals, Phys. Plasmas **16**, 083706 (2009).
[99] L. Couëdel, S. K. Zhdanov, A. V. Ivlev, V. Nosenko, H. M. Thomas, and G. E. Morfill, Wave mode coupling due to plasma wakes in two-dimensional plasma crystals: In-depth view, Phys. Plasmas **18**, 083707 (2011).
[100] T. B. Röcker, A. V. Ivlev, R. Kompaneets, and G. E. Morfill, Mode coupling in two-dimensional plasma crystals: Role of the wake model, Phys. Plasmas **19**, 033708 (2012).
[101] A. Melzer, Connecting the wakefield instabilities in dusty plasmas, Phys. Rev. E **90**, 053103 (2014).
[102] D. A. Kolotinskii, V. S. Nikolaev, and A. V. Timofeev, Effect of structural inhomogeneity and nonreciprocal effects in the interaction of macroparticles on the dynamic properties of a dusty plasma monolayer, JETP Lett. **113**, 510 (2021).
[103] O. S. Vaulina, A. P. Nefedov, O. F. Petrov, and V. E. Fortov, Instability of plasma-dust systems with a macroparticle charge gradient, J. Exp. Theor. Phys. **91**, 1147 (2000).
[104] A. V. Ivlev, U. Konopka, and G. Morfill, Influence of charge variation on particle oscillations in the plasma sheath, Phys. Rev. E **62**, 2739 (2000).
[105] O. S. Vaulina, A. A. Samarian, B. James, O. F. Petrov, and V. E. Fortov, Analysis of macroparticle charging in the near-electrode layer of a high-frequency capacitive discharge, J. Exp. Theor. Phys. **96**, 1037 (2003).
[106] O. S. Vaulina, Stochastic motion of grains with charge gradients in external electric fields, EPL **115**, 10007 (2016).
[107] G. E. Norman, V. V. Stegailov, and A. V. Timofeev, Anomalous kinetic energy of a system of dust particles in a gas discharge plasma, J. Exp. Theor. Phys. **113**, 887 (2011).
[108] J. Kong, K. Qiao, L. S. Matthews, and T. W. Hyde, Temperature measurement of a dust particle in a rf plasma GEC reference cell, J. Plasma Phys. **82**, 905820505 (2016).
[109] M. Rubin-Zuzic, V. Nosenko, S. Zhdanov, A. Ivlev, H. Thomas, S. Khrapak, and L. Couedel, Single particle dynamics in a radio-frequency produced plasma sheath, in *Diverse World of Dusty Plasmas*, AIP Conf. Proc. No. 1925 (AIP, Melville, NY, 2018), p. 020023.
[110] V. Fortov, A. Ivlev, S. Khrapak, A. Khrapak, and G. Morfill, Complex (dusty) plasmas: Current status, open issues, perspectives, Phys. Rep. **421**, 1 (2005).
[111] O. S. Vaulina, S. A. Khrapak, A. P. Nefedov, and O. F. Petrov, Charge-fluctuation-induced heating of dust particles in a plasma, Phys. Rev. E **60**, 5959 (1999).
[112] C. Cui and J. Goree, Fluctuations of the charge on a dust grain in a plasma, IEEE Trans. Plasma Sci. **22**, 151 (1994).
[113] T. Matsoukas, M. Russell, and M. Smith, Stochastic charge fluctuations in dusty plasmas, J Vac. Sci. Technol., A **14**, 624 (1996).
[114] O. Bystrenko, T. Bystrenko, and A. Zagorodny, Charge fluctuations of a dust grain embedded in a weakly ionized gas, Phys. Lett. A **329**, 83 (2004).
[115] S. Ghosh and P. K. Shukla, Dynamical behaviour of stochastic dust charge fluctuations, Phys. Lett. A **376**, 2552 (2012).
[116] B. Shotorban, Stochastic fluctuations of dust particle charge in rf discharges, Phys. Plasmas **19**, 053702 (2012).
[117] A. Piel and C. Schmidt, Dust charging and charge fluctuations in a weakly collisional radio-frequency sheath at low pressure, Phys. Plasmas **22**, 053701 (2015).
[118] P. S. Epstein, On the resistance experienced by spheres in their motion through gases, Phys. Rev. **23**, 710 (1924).
[119] D. Poole, *Linear Algebra: A Modern Introduction*, 4th ed. (Cengage Learning, Stamford, CT, 2015).